Redox Biology 59 (2023) 102565

Contents lists available at ScienceDirect

Redox Biology

journal homepage: www.elsevier.com/locate/redox

Xenobiotic-induced ribosomal stress compromises dysbiotic gut barrier aging: A one health perspective

Junjie Sun [a,1], Juil Kim [a,1], Hoyoung Jeong [a,1], Dasom Kwon [a], Yuseok Moon [a,b,*]

[a] Laboratory of Mucosal Exposome and Biomodulation, Department of Integrative Biomedical Sciences and Biomedical Research Institute, Pusan National University, Yangsan, 50612, South Korea
[b] Graduate Program of Genomic Data Sciences, Pusan National University, Yangsan, 50612, South Korea

ARTICLE INFO

Keywords:
Gut aging
Ribosomal stress
Deoxynivalenol
Gut barrier
Microbiota

ABSTRACT

Upon exposure to internal or environmental insults, ribosomes stand sentinel. In particular, stress-driven dysregulation of ribosomal homeostasis is a potent trigger of adverse outcomes in mammalians. The present study assessed whether the ribosomal insult affects the aging process via the regulation of sentinel organs such as the gut. Analyses of the human aging dataset demonstrated that elevated features of ribosomal stress are inversely linked to barrier maintenance biomarkers during the aging process. Ribosome-insulted worms displayed reduced lifespan, which was associated with the disruption of gut barriers. Mechanistically, ribosomal stress-activated Sek-1/p38 signaling, a central platform of ribosomal stress responses, counteracted the gut barrier deterioration through the maintenance of the gut barrier, which was consistent with the results in a murine insult model. However, since the gut-protective p38 signaling was attenuated with aging, the ribosomal stress-induced distress was exacerbated in the gut epithelia and mucosa of the aged animals, subsequently leading to increased bacterial exposure. Moreover, the bacterial community-based evaluation predicted concomitant increases in the abundance of mucosal sugar utilizers and mucin metabolic enzymes in response to ribosomal insult in the aged host. All of the present evidence on ribosomal insulting against the gut barrier integrity from worms to mammals provides new insights into organelle-associated translational modulation of biological longevity in a one health perspective.

1. Introduction

In response to internal or external stresses, cellular ribosomes stand sentinels. Stress-driven dysregulation of ribosomal integrity triggers eukaryotic translation initiation factor 2 subunit α (eIF2α)-mediated global translational inhibition. In spite of the global translational arrest, the ribosome-inactivating stress (ribosomal stress) triggers the expression of genes important for cellular homeostasis, as well as those integral to a variety of pathogenic processes involved in cell death, inflammation, and other stress responses [1–3]. In particular, humans are inevitably exposed to a specific ribotoxic (28S rRNA-damaging) stressor, deoxynivalenol (DON) which is the most frequently occurring mycotoxin in the global food and environmental systems [4–8]. In addition to DON, other trichothecene mycotoxins, antibiotic anisomycin, and ribosome-inactivating proteins (including ricin, α-sarcin, restrictocin, and shiga toxins) interfere with peptidyl transferase activity by directly or indirectly modifying 28s rRNA at one site in the α-sarcin/ricin loop (A4256) or two other sites (A3560 and A4045) in the peptidyl transferase center [9–11]. This modification leads to peptidyl transferase dysfunction and subsequent global translational arrest [12–15]. Mechanistically, damages in the structure and functionality of 28S ribosomal RNA during gene translation lead to homeostatic or pathogenic cellular reprogramming via intracellular sentinel signaling pathways, which include mitogen-activated protein kinase (MAPK)-linked signaling cascades as the primary platform in mammalian cells [1,16,17]. The 28S rRNA damage facilitates ribosomal binding to dsRNA-binding domains of protein kinase R (PKR) and induces enzymatic activation [18]. Following exposure to high levels of ribosomal stressors, activated PKR modulates stress-induced cell death processes via activation of MAPKs such as *c*-Jun N-terminal kinase 1 and 2 [19]. In contrast, low levels of exposure to the ribosomal insults may promote the expression of adaptive stress-responsive genes including pro-inflammatory genes via

* Corresponding author. Department of Integrative Biomedical Sciences, Pusan National University, Yangsan, 50612, South Korea.
E-mail address: moon@pnu.edu (Y. Moon).
[1] Authors equally contributed to the present study.

https://doi.org/10.1016/j.redox.2022.102565
Received 26 October 2022; Received in revised form 28 November 2022; Accepted 28 November 2022
Available online 30 November 2022
2213-2317/© 2022 The Authors. Published by Elsevier B.V. This is an open access article under the CC BY-NC-ND license (http://creativecommons.org/licenses/by-nc-nd/4.0/).

PKR-mediated ribosomal recruitment and activation of MAPKs such as p38 [16,18]. The ribosomal 40S subunit serves as a scaffold for PKR under the ribosomal stress, which facilitates p38 mobilization and activation for target gene induction despite the global translational arrest. Such stress-sentinel pathways by ribosomal inactivation are potent etiological factors involved in epithelial inflammatory or malignant distress including inflammatory bowel diseases (IBD) and colorectal cancer in the experimental models [20–25]. Moreover, epidemiological studies suggest potent associations between ribosome-inactivating stress and human gastrointestinal illness [17,26–28].

Gastrointestinal epithelium is a sentinel line against pathogens and participates in the maintenance of host integrity and is imprinted with accumulated environmental and dietary insults which can damage the gut and other organs via circulation. Disruption of gut epithelial barrier integrity can allow increased translocation of noxious microbes and substances across the intestinal barrier, leading to a greater risk of systemic infection, inflammation, and sepsis. The aging process can alter the integrity of the gut barrier and increase vulnerability to GI disorders. In particular, disorders of the gastrointestinal (GI) tract are particularly common in the elderly population, which may contribute to the overall vulnerability to sepsis-linked mortality in hosts with poor defenses [29]. Moreover, the epithelium-based defense in invertebrates, such as *Caenorhabditis elegans*, is important for the generation of evolutionarily conserved aspects of innate immunity, and the maintenance of epithelial integrity is associated with the lifespan of these organisms [30–33]. *C. elegans* are particularly dependent on the gut epithelial layer because they lack specialized leukocytes, such as macrophages and lymphocytes, for defending against pathogens [30,34]. This reduced complexity can be experimentally advantageous for the detailed characterization of innate immune signaling cascades. The present study is based on an assumption that ribosomal dysregulation may affect the lifespan via modulating sentinel organs. In addition to the mammalian aging model, the present study evaluated a gut model of *C. elegans* since it is an evolutionarily conserved responder to both endogenous and environmental stressors. In particular, the stress signaling response from the ribosome was associated with gut distress during the aging process. Our results provide new insights into the roles of ribosomes in the regulation of human longevity and susceptibility to gut-associated chronic diseases.

2. Materials and Methods

2.1. Human transcriptome dataset analysis

The Genotype-Tissue Expression (GTEx, V8) dataset was used for aging-associated gene expression analysis (17,382 sample entities of 54 tissues from 948 donors). RNA-seq raw counts and normalized TPM matrices from the normal transverse colonic tissues were quantified for comparison among different age groups.

2.2. Animal ethics statement

The experimental protocols followed in this study were reviewed and approved by the Animal Ethics Committee of Pusan National University (PNU)-IACUC (PNU-2015-0786 and PNU-2013-0291). The animal study was performed in accordance with the guidelines for animal experiments issued by PNU-IACUC.

2.3. Murine insult experiments: aging rat model

Sprague-Dawley rats (aged 6 and 19 months; N = 6 per group) were purchased from Samtako Bio Korea (Osan, Korea) and acclimated to the animal care facility for 7 days before beginning the experiments. Based on a previous report [35], animals were housed in an air-conditioned environment under a 12 h light/dark cycle and were given ad libitum access to standard rodent chow (Samtako) and water. Food intake and body weight were monitored every 5–8 days. The rats were euthanized, tissues collected, and perfusion was immediately fixed. Formalin-fixed and paraffin-embedded sections (thickness, 5 μm) were prepared from the small intestine. Slides were stored at room temperature until analysis.

2.4. Murine insult experiments: mouse model

Male C57BL/6 young (6 weeks) and old (19 months) mice from the Korean Distributor of Taconic Biosciences (DBL, Eumseong, Korea) were exposed to 25 mg/kg of DON for 12 h by oral gavage and then killed. Male C57BL/6 mice (8 weeks old) were caged in groups of 3–4 mice, and the cages were changed weekly. Briefly, mice were inoculated intragastrically with streptomycin sulfate (single dose, 10 mg per mouse) to selectively eliminate intestinal facultative anaerobic bacteria. After 22 h, the mice were inoculated with phosphate-buffered saline (PBS) or p38 inhibitor (SB203580, 10 mg/kg) by intraperitoneal (I.P.) injection. After a further 2 h, the mice were inoculated intragastrically with either PBS or DON (25 mg/kg). After 24 h, the mice were inoculated intragastrically with either sterile LB broth or EPEC bacteria (1×10^9 CFU). The mice were killed on the day 4 after bacterial inoculation, and their tissues were fixed in Carnoy's solution.

2.5. Histological assessment

Hematoxylin and eosin staining was performed using standard procedures described in our previous reports [36,37]. Scoring of disease severity was based on the following four parameters. Inflammatory cell infiltration was scored as follows: 0, rare inflammatory cells in the lamina propria; 1, increased numbers of granulocytes in the lamina propria; 2, confluence of inflammatory cells extending into the submucosa; and 3, transmural extension of the inflammatory infiltrate. Crypt damage was scored as follows: 0, intact crypts; 1, loss of the basal half; 2, entire crypt loss; and 3, confluent erosion. Ulceration was scored as follows: 0, absence of ulcer; 1, one or two foci of ulcerations; 2, three or four foci of ulcerations; and 3, confluent or extensive ulceration. Edema was scored as follows: 0, absence of edema; 1, mild; 2, moderate; and 3, severe.

2.6. Immunohistochemistry

Methods are based on our previous reports [37–39]. Before immunostaining, formalin-fixed paraffin-embedded tissues from mouse intestines were sectioned (5 μm), deparaffinized, and rehydrated. Tissue slides were heated in 10 mM sodium acetate (pH 6.0) for 5 min at 121 °C for antigen retrieval and were bathed in a 0.3% H_2O_2-PBS solution for 15 min at room temperature in the dark to quench endogenous peroxidase. After the samples were washed with Tris-HCl-Tween 0.5%, tissue sections (5 μm) were blocked with 5% fetal bovine serum in PBS, incubated in a 1:250 dilution of primary antibody overnight at 4 °C, and repeatedly washed using PBS. The primary antibodies used were anti-p-p38 (1:1000 dilution; Santa Cruz Biotechnology, Santa Cruz, CA) and anti-lysozyme (1:250 dilution, Biobyt, Cambridge, UK). The samples were incubated with secondary horseradish peroxidase-conjugated anti-mouse or anti-rabbit IgG antibody (1:250 dilution; Enzo Life Sciences, Inc. Farmingdale, NY, USA) for 2 h at room temperature and were subjected to repeated washing with PBS. Bound antibodies were identified by incubation for 10 min with freshly prepared substrate buffer (0.05% diaminobenzidine [DAB; Sigma-Aldrich Chemical Co.] and 0.015% H_2O_2 in PBS). After a final wash in PBS and dH_2O, the slides were counterstained with Mayer's hematoxylin for 5 min and dehydrated in a graded alcohol series (50%, 70%, 80%, 90%, 95%, 100%, and 100%). The sections were then examined at various magnifications using an Axio Imager (Carl Zeiss MicroImaging, GmbH, Oberkochen, Germany). To analyze the proportion of positively stained cells in the tissue, at least four representative areas were measured by computer-assisted analysis using HistoQuest image analysis software

version 4.0 (TissueGnostics, Vienna, Austria). The pixels of images viewed in this software are converted to grayscale and assigned an arbitrary number relating to staining intensity. HistoQuest image analysis software differentiates hematoxylin-positive and diaminobenzidine (DAB)-positive cells or areas that are recorded as events (cells/nuclei) or area of staining. The results allow determination of "how many cells express how much of a given marker". Values were optimized by counting the numbers of DAB-positive events and hematoxylin-positive events. The graphs statistically compare the values among groups.

2.7. Immunofluorescence staining of murine tissues

Methods are based on our previous reports [37–39]. Small intestine samples were dehydrated, embedded in paraffin, and sliced into 5 μm sections for immunofluorescence analysis. Before immunostaining, formalin-fixed paraffin-embedded small intestines were sectioned (5 μm), deparaffinized, and rehydrated. Tissue slides were heated in 10 mM sodium acetate (pH 9.0) for 5 min at 121 °C for antigen retrieval and bathed in 3% H_2O_2-PBS solution for 15 min at room temperature in the dark to quench endogenous peroxidase. After washing with 0.5% Tris-HCl-Tween, tissue sections were blocked with 3% fetal bovine serum in PBS with Tween 20 (PBST) and incubated with anti-mouse claudin 3 (CLDN3) antibody (1:200, Santa Cruz) at 4 °C overnight. Samples were then washed in PBST, incubated with 488-conjugated goat anti-mouse IgG (Bethyl Laboratories, Montgomery, TX, USA) for 2 h at room temperature, washed again in PBST, dehydrated through a graded alcohol series (50%, 70%, 80%, 90%, 95%, 100%, and 100%), and mounted in DAPI-containing mounting medium. Sections were examined at various magnifications using a fluorescence microscope (Eclipse Ts2R, Nikon, Tokyo, Japan).

2.8. Alcian blue (AB) staining of murine tissues

Methods are based on our previous reports [37,38]. For AB staining, sections were deparaffinized in xylene, rehydrated in ethanol, and incubated in dH_2O for 5 min. AB 8GX (Biosesang Company) was applied to sections for 30 min at room temperature, followed by a 2 min wash under running tap water, and counterstaining with Nuclear Fast Red or hematoxylin. Stained sections were rapidly dehydrated in two changes of 95% ethanol, followed by two changes of absolute alcohol, cleared in xylene, and mounted in a synthetic mountant (Thermo Fisher Scientific, Seoul, Korea).

2.9. Gram staining of murine tissues

Gram staining was performed as follows: tissue sections were deparaffinized in xylene, rehydrated in ethanol, incubated in dH_2O for 5 min, stained for 1 min using crystal violet, and then washed under tap water [37,39]. Slides were then stained with Gram's iodine for 1 min, rinsed under tap water, dipped in 95% ethyl alcohol for 5–10 s, and rinsed again under tap water. The slides were stained again for 1–2 min in safranin and rinsed under tap water. Stained sections were rapidly dehydrated in two changes of 95% ethanol, followed by two changes of absolute alcohol, cleared in xylene, and mounted in a synthetic mountant (Thermo Fisher Scientific, Korea). The safranin stains decolorized gram-negative cells red/pink, while the gram-positive bacteria remained blue.

2.10. Gut epithelial F-actin staining

Paraffin sections were treated in xylene and rehydrated in an ethanol and water gradient. To detect F-actin, sections were incubated with tetramethyl rhodamine B isothiocyanate-conjugated phalloidin (0.5 μg/ml, Sigma-Aldrich, USA) for 2 h in the dark [37]. Sections were then washed and counterstained with DAPI to detect nucleic acid.

2.11. Fluorometric assay of FITC-conjugated dextran in vivo

Methods are based on our previous reports [37,38]. Intestinal permeability was evaluated in different groups of mice using orally administered permeability marker FITC-conjugated dextran dissolved in water (4 kDa, 50 mg/ml; Sigma-Aldrich) as described in our previous report [37]. The blood serum was collected 3 h later, and the serum concentration of FITC-conjugated dextran was determined using a plate reader (SpectraMAX M2e, Molecular Devices, Sunnyvale, CA, USA). The sample emission spectrum (535 nm) was recorded after excitation at 490 nm. The concentration of FITC-conjugated dextran in the serum was determined using a FITC-dextran standard curve.

2.12. Barrier integrity assessment in the intestinal epithelial cell monolayer

For the measurement of TEER based on the previous study [40], intestinal porcine epithelial cell line-1 (IPEC-1; Leibniz Institute DSMZ-German Collection of Microorganisms and Cell Cultures, Braunschweig, Germany) was seeded at a density of 4×10^5 per well in 24-well transwell filters with 0.4 μm pores (Becton-Dickinson Labware, Franklin Lakes, NJ, USA). The cells reached confluence within 2 days. For cell differentiation, complete DMEM/F-12 media containing 100 nM dexamethasone was used and changed every other day until complete differentiation [41]. At the end of the differentiation process (on the 10th day after the addition of dexamethasone), cells were treated with 1000 ng/ml DON. TEER was measured every 12 h using an EVOM2 epithelial voltohmmeter (World Precision Instruments, Sarasota, FL, USA). Experimental TEER values were expressed as Ω cm^2. All measurements were performed in triplicate. For the paracellular tracer flux assay based on the previous report [40], differentiated IPEC-1 in 0.4 μm pore inserts (generated as described above) were treated with 1000 ng/ml DON for 48 h. Next, 4 kDa FITC-dextran (Sigma-Aldrich Chemical Company) was dissolved in cell culture medium and added to the apical compartment with enterocytes at a final concentration of 2.2 mg/ml. After 1 h of incubation, the amount of fluorescence in the basolateral compartment was measured using a Victor3 fluorometer (PerkinElmer, Waltham, MA, USA). The excitation and emission wavelengths were 490 and 535 nm, respectively. Data presented are representative of three independent experiments [42].

2.13. Worm culture conditions

Methods for maintenance of *C. elegans* are based on our previous reports [37,38]. *C. elegans* Bristol N2 (Brenner 1974) and the mutant strains (AU1 [*ag1*, *sek-1*, homolog MAPKKK] and pmk-1 [*km25*]) (*Caenorhabditis* Genetics Center, University of Minnesota, Minneapolis, MN, USA), were maintained at 20–25 °C on nematode growth medium (NGM) agar (50 mM NaCl, 1.7% Agar, 0.25% peptone, 1 mM $CaCl_2$, 5 μg/ml of cholesterol, 1 mM $MgSO_4$, and 25 mM KPO_4 in distilled H_2O [dH_2O]) plates spread with *Escherichia coli* OP50 as a food source [37,38]. *C. elegans* were synchronized with a mixture of 500 μl 5 N NaOH, 1 ml 5% solution of sodium hypochlorite (Yohanclorox, Seoul, Korea), and 3.5 ml autoclaved dH_2O. Synchronized eggs were seeded on NGM agar plates for growth, and worms at the L4 stage were seeded on new NGM agar plates spread with chemicals of interest (see below) and *E. coli* OP50 (OD_{600} = 0.6). To prepare *C. elegans* media for experimental treatments, chemicals were added to *E. coli* OP50 culture media, which was spread on the culture dishes. For lifespan assays, 30 synchronized worms were grown on NGM agar plates spread with *E. coli* OP50 with chemicals at 24 °C. The surviving worms that moved in response to touch with a platinum wire were scored each day. To prevent progeny production, worms were transferred to new NGM plates every 2 days.

2.14. Bacterial colonization assay in the worms

To prepare for bacterial colonization assays, the worms were age-synchronized by bleaching, and embryos were incubated at 24 °C on NGM plates containing *E. coli* OP50 until the L4 stage, as previous described [37,38]. After exposure to DON for 48 h, 10 worms were selected and placed into a 2 ml tube containing 25 mM levamisole to induce paralysis and inhibit pharyngeal pumping. Then, LM buffer (25 mM levamisole in M9 buffer) containing 100 μg/ml gentamicin was added, followed by incubation for 45 min to remove the surface bacteria. The worms were then washed three times in LM buffer to remove bacteria and antibiotics. The washed worms were incubated with 1% Triton X-100 and mechanically disrupted using a motor pestle for 3 min. Worm lysates were diluted in M9 buffer, spread on Luria-Bertani (LB) agar containing 50 μg/ml streptomycin, and incubated overnight at 37 °C. Colonies were quantified, and the number of bacteria per nematode was calculated. For the fluorescence visualization, *E. coli* OP50 were transformed with the GFP-UV vector (which is resistant to Ampicillin, 100 μg/ml) for bacterial colonization assays [37,38]. The intestinal GFP-UV-OP50 fluorescence of worms was examined by fluorescence microscopy using an Axio Imager M2 (ZEISS, Gottingen, Germany). The Multi Gauge V. 3.0 (Fusifilm Life Science, USA) program was used to measure intestinal GFP-OP50, bacterial distribution, and width and length of the intestines.

2.15. Intestinal barrier function assay (Smurf assay)

Methods for *C. elegans* are based on our previous reports [37,38]. After 24 h DON treatment, worms from the NGM agar plates were cultured for 3 h in the liquid media of UV-killed *E. coli* OP50 that was mixed with blue food dye (TCI, FD&C Blue #1, B0790, Portland, OR, USA; 5.0% wt/vol in NGM liquid solution). The worms were then washed in M9 buffer until the blue color was no longer visible and were anesthetized in M9 buffer containing 25 mM levamisole. The worms were then analyzed on a slide to determine the presence of blue food dye in the body cavity by using an Eclipse Ts2R microscope (Nikon, Tokyo, Japan) under 20 × magnification. Data were analyzed using GraphPad Prism software.

2.16. DAPI staining of worms

The worms washed in M9 buffer were mounted on slides. After wiping away surplus liquid using Whatman paper, 95% ethanol was added and allowed to dry. This procedure was repeated four times. The fixed worms were then added to fluorescent mounting medium containing DAPI solution (IHC World, Woodstock, MD, USA).

2.17. Quantitative PCR (qPCR)

qPCR was conducted using a Rotor Gene Q instrument (Qiagen, Hilden, Germany) to measure the amplification of cDNA using SYBR green (Enzynomics) based on the previous report [38]. All experiments included three replicates to ensure reproducibility, and each independent experiment was repeated three times. Relative quantification of gene expression was performed using the comparative threshold cycle (Ct) method. The Ct value is defined as the point where a significant increase in fluorescence is observed. The 5′ forward and 3′ reverse complement PCR primers for amplifying each gene were as follows: Act-1 (forward 5′-CCA AGA GAG GTA TCC TTA CC-3′, reverse 5′CTT GGA TGG CGA CAT ACA TG-3′), lys-7 (forward 5′- CGT CAA ACT TGG CAT CTT AT-3′, reverse 5′-CGT TAT TTG GCC AGT TAG TT-3′), T24B8.5 (forward 5′- TCA TCG GAT TTG TGA TTG TG-3′, reverse 5′-GTC TAA CAT AGT TTG GGC AG-3′), and lys-8 (forward 5′-AAA TCA GTG GCT CTT TTG TC-3′, reverse 5′-CAT GTA GAT CTC TGT TCC GA-3′).

2.18. Stool sample collection and DNA extraction

After 24 h of DON administration, stool samples (5–6 pieces) (100 mg) of fecal samples were collected before animal sacrifice. The collected stool samples were stored at −150 °C prior to DNA extraction. Microbial DNA was extracted and purified from 100 mg of the fecal sample using Exgene Stool DNA mini kit (GeneALL, Seoul, Korea) according to the manufacturer's instructions. The extracted DNA was quantified using Qubit fluorometer and a high-sensitivity dsDNA reagent kit (Invitrogen, Carlsbad, CA, USA).

2.19. Amplification of the 16S rRNA genes and library preparation

A total DNA samples were pooled as treatment groups for a 16S metagenomic library preparation. The V4 region of the 16S rRNA genes was PCR-amplified with a primer set (533F, 5′-GTGCCAGCMGCCGCGGTAA-3'; 806R, 5′-GACTACHVGGGTWTCTAAT-3′) and Illumina sequencing adaptors (Illumina Inc.) using the KAPA HiFi HotStart Ready Mix (KAPA Biosystems, Wilmington, WA, USA) under the following cycling conditions: initial denaturation 95 °C for 3 min, followed by 25 cycles of denaturation at 95 °C for 30 s, annealing at 55 °C for 30 s, extension at 72 °C for 30 s, and a final extension at 72 °C for 5 min. After amplicon purification using AMPure® XP beads (Agencourt Biosciences, Beverly, MA), PCR products were validated for library size using a BioAnalyzer. Then, the PCR amplicon was subjected to indexing PCR using the Nextera XT Index Kit (Illumina, Inc.). The PCR cycling conditions were as follows: 95 °C for 3 min, followed by 8 cycles of denaturation at 95 °C for 30 s, annealing at 55 °C for 30 s, extension at 72 °C for 30 s, and a final extension at 72 °C for 5 min. The indexed PCR amplicons were purified using AMPure® XP beads, verified for size using a BioAnalyzer, and quantified using the Qubit fluorometer. The quantified amplicons were diluted to 1 nM and pooled together for sequencing on an Illumina iSeq platform (Illumina, Inc.), targeting 2 × 150 bp paired-end sequence reads.

2.20. Microbiome data processing

All sequences were quality-filtered and the primers were trimmed using Trimmomatic (v0.39) [43] with the following parameters: LEADING:3 TRAILING:3 MINLEN:36 SLIDINGWINDOW:4:15). The read pairs passing the quality filter were further analyzed using the Quantitative Insights Into Microbial Ecology 2 (QIIME2, v2020.2) pipeline [44]. Using the DADA2 algorithm [45], the 34 bases of the reverse reads were truncated for quality improvement. The read pairs were then joined, denoised, and dereplicated, and chimeras were removed. The detailed data were used to call ASVs. The 16S rRNA representative sequences were assigned to taxonomic groups using the QIIME2 naive Bayes classifier trained on 99% operational taxonomic units (OTUs) and the primer region from the SILVA rRNA database (v132) [46]. The taxonomic classification was visualized using the QIIME2 taxon barplot plugin. The 16S rRNA representative sequences were subjected to masked multisequence alignment using MAFFT [47,48]. A phylogenetic tree was constructed using FastTree [49]. A heatmap, depicting the percentage abundance of OTUs, the relative abundance of which was in the top 30 in any sample, was generated using the R package, QIIME2R (v0.99.22). A phylogenetic tree based on the abundant OTUs was constructed and visualized using the neighbor-joining algorithm with Jukes-Cantor correction using MEGA X [50]. Additionally, we used the CLcommunity™ software for analysis.

2.21. Statistics and reproducibility

Statistical analyses were performed using GraphPad Prism v. 8.4.2 (La Jolla, CA, USA). For comparative analysis of two groups of data, Student's *t*-test was performed. For comparative analysis of multiple groups, data were subjected to analysis of variance (ANOVA) with

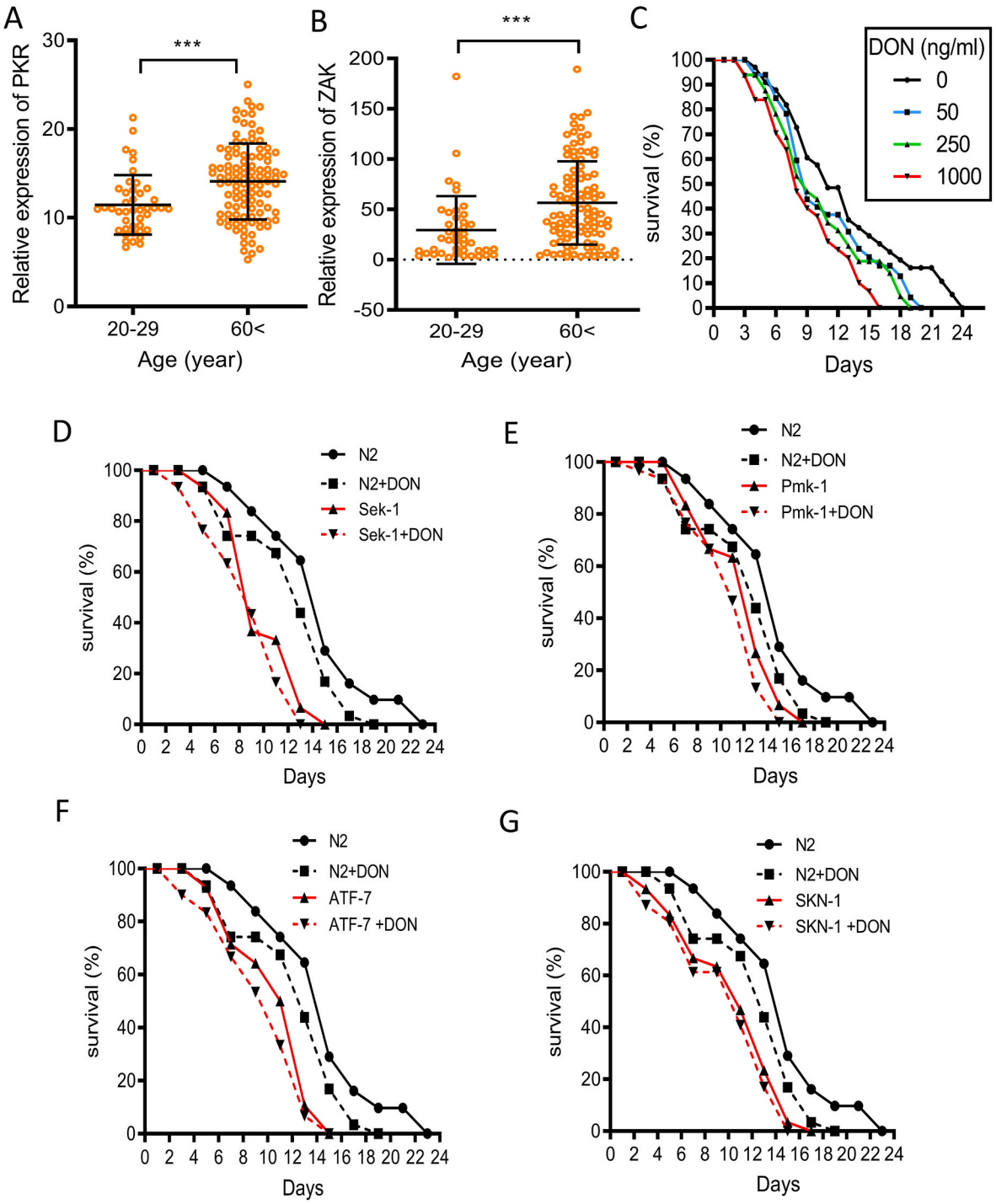

Fig. 1. Involvement of the ribotoxic stress response and signaling in the aging process

A-B. Expression of ribotoxic stress-responsive genes (PKR (A), ZAK (B)) were assessed in young and elderly subjects (GTEx V8, n = 148). Results are shown as mean values ± SD. Asterisks (*) indicate significant differences between groups (***$p < 0.001$). **C.** Survival of wild-type (N2) *C. elegans* grown on lawns of *E. coli* OP50 containing different concentrations of DON. Age-synchronized young-adult worms were supplemented with different doses of DON, and the survival of the worms was monitored three times a day until all worms were dead. **D-G.** Survival of wild-type (N2), *Sek-1* mutant (D), *Pmk-1* mutant (Pmk-1 MT, E), *ATF-7* mutant (ATF-7 MT, F), and *SKN-1* mutant (SKN-1 MT, G) *C. elegans* exposed to vehicle or the ribotoxic stressor (500 ng/ml DON).

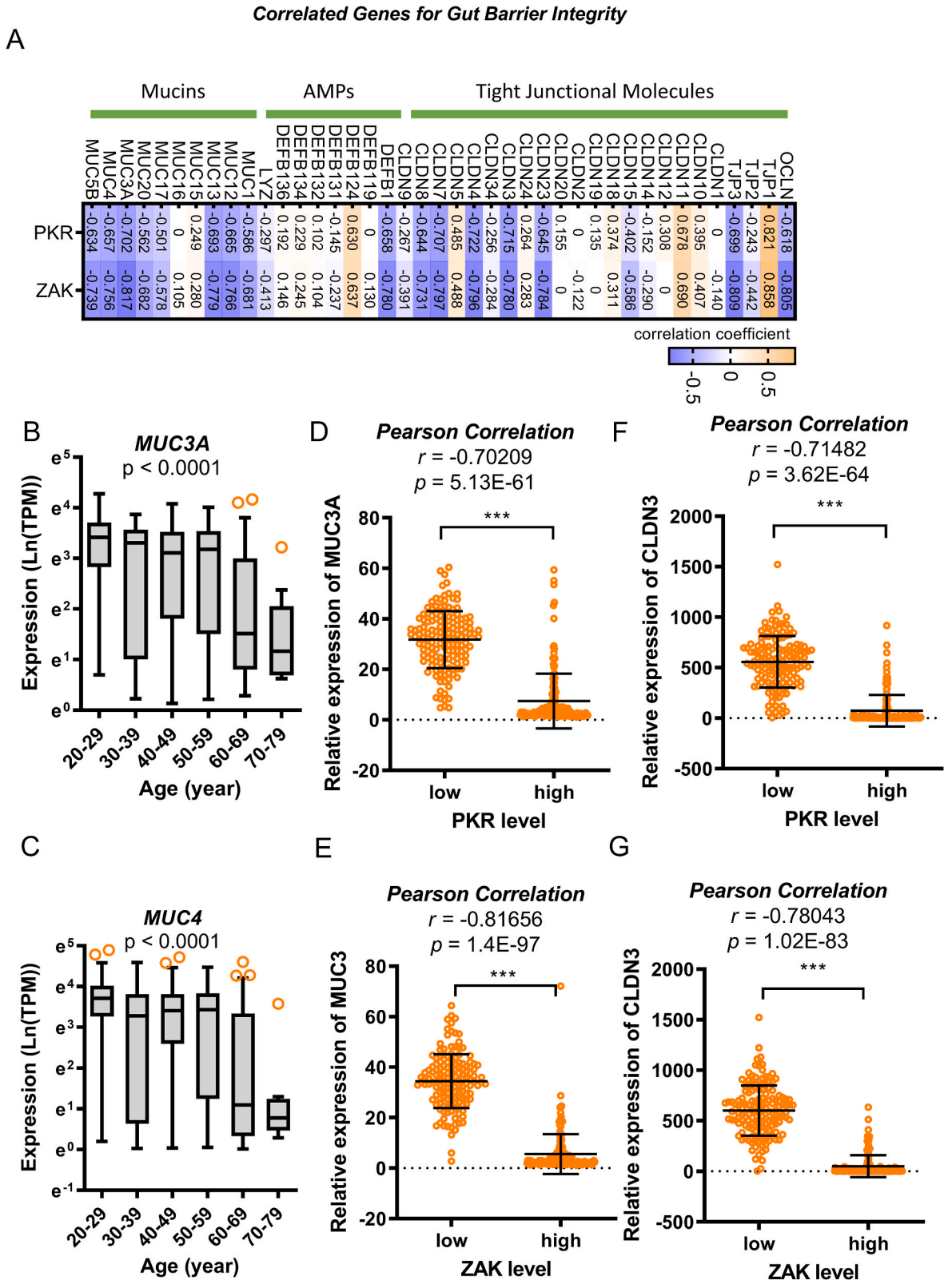

Fig. 2. Human intestinal transcriptome-based evaluations

A. Correlation of the ribosomal stress markers and gut barrier integrity-linked molecules in the nondiseased human population (GTEx dataset v8). For two gene correlation coefficient (R) determination in the IBD-based datasets, *Pearson*'s correlation analysis was performed. **B–C.** Results are depicted as box-and-whisker plots (Tukey) for expression of mucins (*MUC3A or MUC4*) in normal mucosal intestinal tissues (GTEx dataset v8). Values are presented as transcripts per million (TPM). Statistical significance of the expression variation with age is illustrated on the top of each plot (*Kruskal–Wallis* test). **D-G.** Based on PKR (D, F), or ZAK (E,G) levels, we chose the 150 highest and 150 lowest level samples, which were further evaluated for MUC3A or CLDN3 levels. Results are shown as mean values ± SD and asterisks (*) indicate significant differences between groups (***p < 0.001).

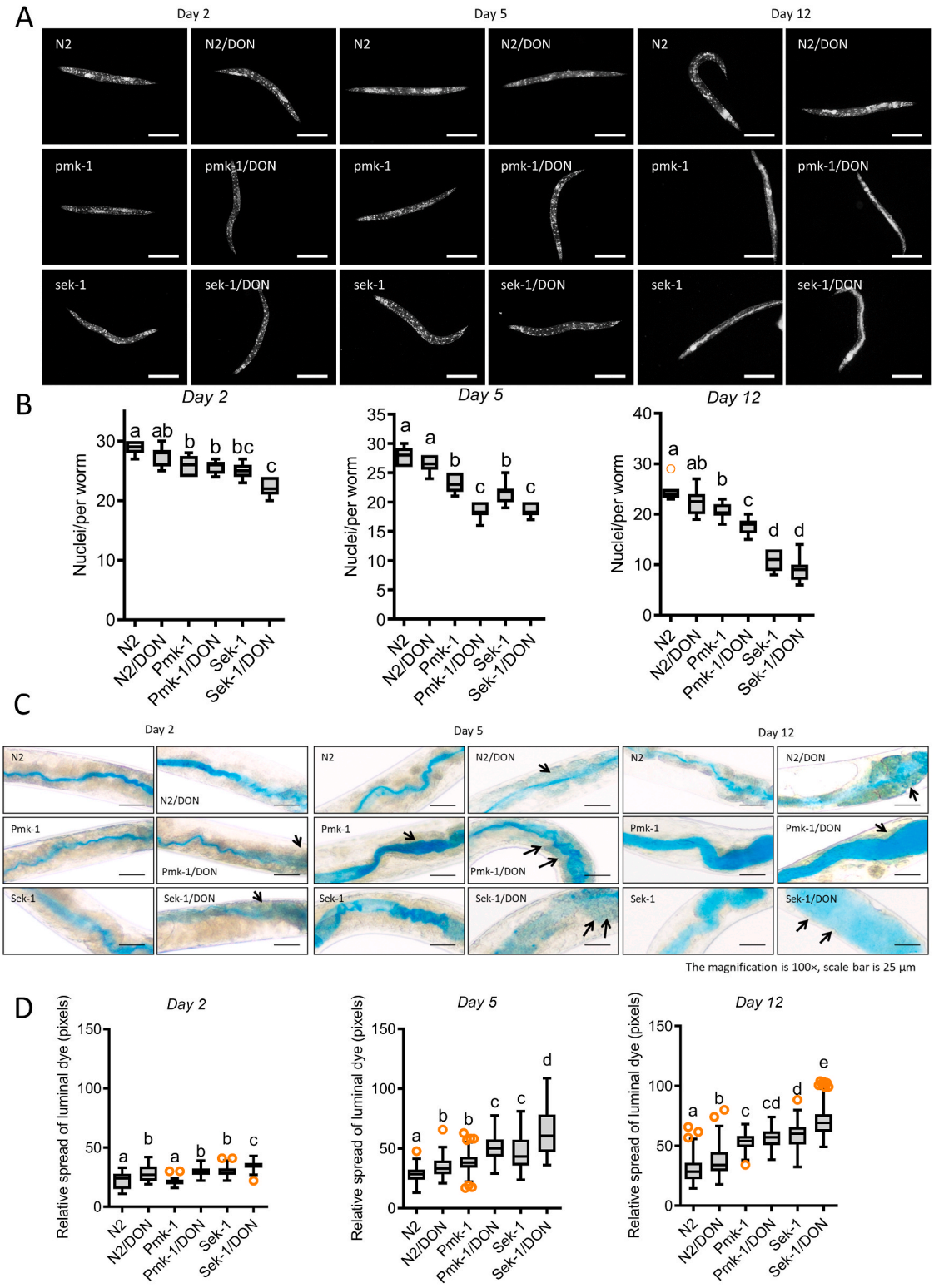

Fig. 3. Ribosomal insult disrupts the integrity of the worm gut barrier

A-B. To visualize intestinal cell nuclei, *C. elegans* of different ages were treated with vehicle or the ribosomal stressor (500 ng/ml DON) for 24 h and stained with DAPI (blue) (A, × 100; scale bar(s), 100 μm). The graphs indicate the number of intestinal nuclei in worms exposed to the ribosomal stressor at different ages (B). Results are shown as a plot with Tukey whiskers. Different letters over each box represent significant differences between groups ($p < 0.05$). **C-D.** Representative images of N2, *Sek-1*, *Pmk-1* mutant animals after 3 h of staining with blue food dye. Animals were exposed to 24 h of treatment with the vehicle or 500 ng/ml DON (C). Black arrows indicate areas where blue food dye has leaked from the gut lumen into the body cavity, giving rise to the Smurf phenotype. Microscopic analysis was performed at 200 × magnification; scale bar(s), 25 μm. Quantitative analysis of the relative leakage of the dye (D). Results are shown as a plot with Tukey whiskers. Different letters over each box represent significant differences between groups ($p < 0.05$). . (For interpretation of the references to color in this figure legend, the reader is referred to the Web version of this article.)

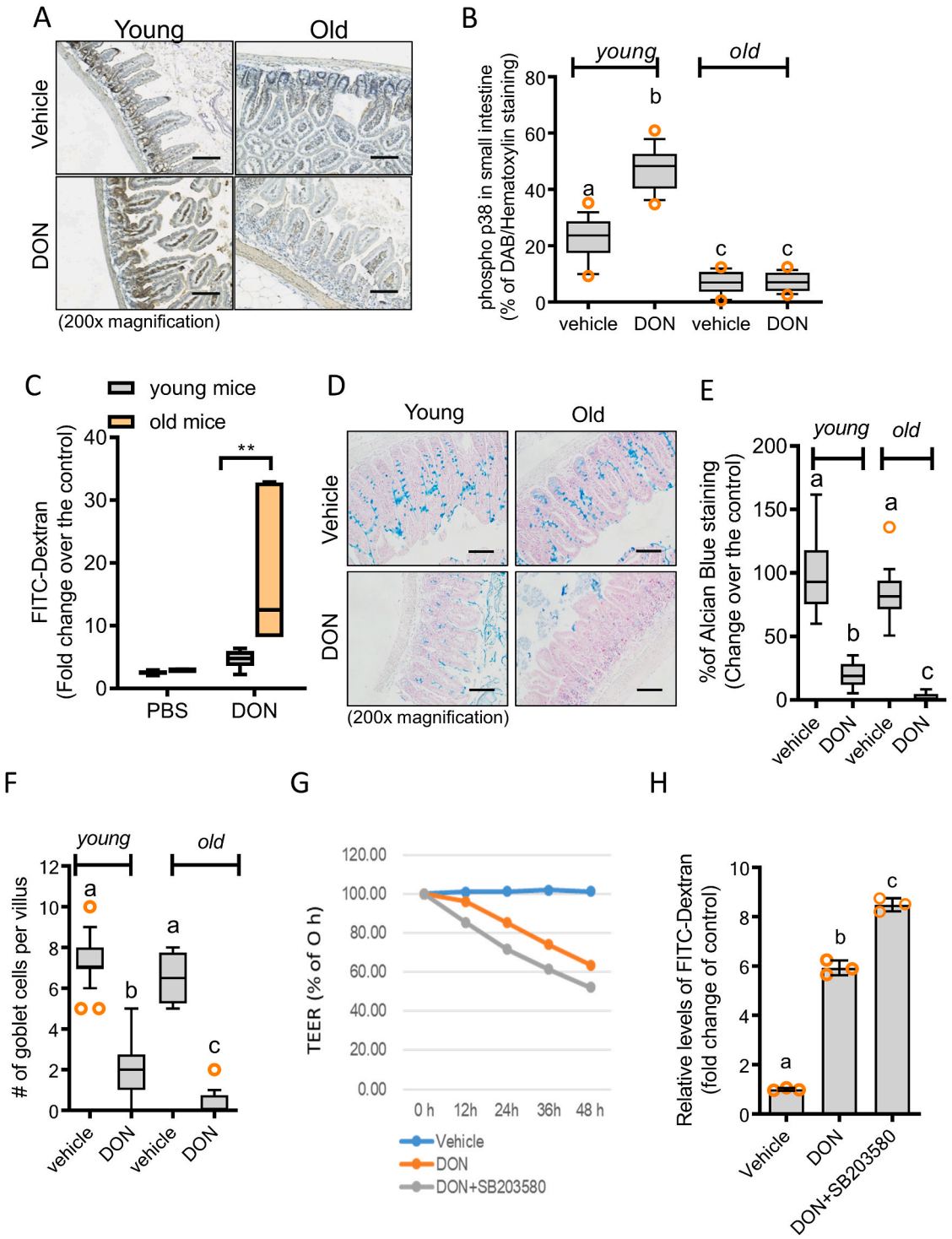

Fig. 4. Ribosomal insult disrupts mucosal and epithelial barriers in mice

A-B. Young (6 weeks) and old (19 months) mice were exposed to chemical ribosomal stressor (25 mg/kg DON) for 12 h (N = 20). Small intestines were stained for immunohistochemistry using anti-p-p38 antibody with hematoxylin counterstaining (A), and expression levels were quantified using Histoquest analysis software (× 200; scale bar(s), 100 μm) (B). Results are shown as a plot with Tukey whiskers. Different letters over each box represent significant differences between groups ($p < 0.05$). **C.** FITC-dextran concentration in blood samples from C57BL/6 mice exposed to vehicle or chemical ribosomal stressor (25 mg/kg DON) for 3 h (**$p < 0.01$, N = 6). Results are shown as a plot with Tukey whiskers. Asterisks represent a significant difference between groups ($p < 0.05$). **D-F.** Young (6 weeks) and old (19 months) mice were exposed to vehicle or chemical ribosomal stressor (25 mg/kg DON) for 12 h (N = 20). Small intestines were isolated for the analysis of goblet cells and mucin production, which was visualized by staining with alcian blue (× 200; scale bar(s), 100 μm) (D), and expression levels were quantified using Histoquest analysis software (E). Additionally, the numbers of the goblet cells per villus were compared in each group (F). Results are shown as a plot with Tukey whiskers. Different letters over each box represent significant differences between groups ($p < 0.05$). **G-H.** Epithelial permeability of differentiated IPEC-1 cells exposed to each combination of chemicals at different time points using TEER (G) and FITC-dextran (H). Different letters over each bar represent significant differences between groups ($p < 0.05$). Data represent three independent experiments. (For interpretation of the references to color in this figure legend, the reader is referred to the Web version of this article.)

Newman-Keuls method as a *post hoc* ANOVA assessment. For two gene correlation coefficient (R) determination in IBD-based datasets, *Pearson*'s correlation analysis was performed. All *in vitro* evaluations are representative of two or three independent experiments. Details of the number of biological replicates and the assays are given in each figure legends.

3. Results

3.1. Effect of ribosomal stress on the lifespan of C. elegans under the ribosomal stress

Ribosomal stress responses were assessed in human aging using the transcriptome dataset of nondiseased tissue from the Genotype-Tissue Expression (GTEx) project. We assessed key sentinel molecules in response to ribosomal dysfunction in the gut. In particular, protein kinase R (PKR) and leucine-zipper and sterile alpha motif containing kinase (ZAK) are crucial upstream sentinel molecules during ribosomal stress responses [19,51]. Levels of PKR and ZAK transcript expression in elderly subjects were significantly higher than the young subjects (Fig. 1A and B), indicating the ribosomal stress increases with the aging process. Simulative assessment of the aging-associated effects of ribosomal stress was evaluated using *C. elegans* rather than mammalian models, since the average lifespan of a wild-type worm is approximately 3 weeks. In terms of lifespan, the survival of wild-type worms (N2) decreased with exposure to a representative chemical ribosomal stressor (deoxynivalenol, DON) in a dose-dependent manner (Fig. 1C). According to the extensive survey in 7049 cereal samples sourced in North and South Americas, Europe, and Asia during 2009–2011, 59% of samples were contaminated with DON, and an average contamination level was 1 mg DON/kg grain [52]. Therefore, in the present models, we used 50–1000 ng/ml DON which corresponds to mammalian exposure levels (0.05–1.0 mg DON/kg diet), which is supposed to be realistic within the average contamination level [40]. Moreover, epithelial exposure to 50–1000 ng/ml DON increases the proinflammatory cytokine expression in a dose-dependent manner despite ribosomal stress-induced cell cycle arrest [3,53]. In the present study, most of mucosal exposure was performed at 20% cell growth-inhibitory dose of the ribotoxic stressor (ID_{20}, 500 ng/ml DON). In mammalian cells, p38 MAPK signaling is a central signaling mediator of cellular stress responses to ribosomal dysfunction [54–56]. On an assumption that stress-responsive p38 MAPK signaling can be involved in the aging process, it was assessed in the nematode model. The involvement of the p38-activated pathway in the regulation of the lifespan was assessed in *C. elegans* under the ribotoxic stress. *Sek-1* encodes a MAPK kinase (MAPKK) that phosphorylates the p38 MAPK Pmk-1 in *C. elegans*. *Sek-1* and *Pmk-1* mutant animals displayed shortened lifespan compared to the wild-type (N2) in response to the chemical ribosomal insult (Fig. 1D and E, respectively). Moreover, genetic mutation of Pmk-1 downstream signaling transcription factors including *ATF-7* and *SKN-1* also notably reduced the lifespan of the nematode (Fig. 1F and G, respectively). Taken together, these results indicate that the p38 MAPK signaling positively influences the lifespan of worms in both normal and ribotoxic stress states.

3.2. Disruption of gut epithelial and mucosal barriers in intoxicated hosts

Since the aging process is closely associated with deterioration of the gastrointestinal tract as mentioned in the introduction, we analyzed expression levels of human intestinal integrity biomarkers using the transcriptome dataset of nondiseased tissue from GTEx project. It was initially hypothesized that the host ribosomal stress is elevated with aging (Fig. 1A), which will influence the gut barrier integrity during the stress. We specifically evaluated correlation of the ribosomal stress markers (*PKR* and *ZAK*) and levels of components of the mucosal and epithelial layer, including mucins, antimicrobial peptides (AMPs), and tight junction-associated molecules. In particular, among the components, the most of mucins are negatively associated *PKR* and *ZAK* (Fig. 2A). In addition, the ribosomal stress marker levels displayed high correlation with expressions of the main intestinal claudins (*CLDN3, CLDN7, CLDN8*, and *CLDN15*), tight junction protein 3 (*TJP3*), and occludin (*OCLN*). Of note, expression of two mucins (*MUC3A* and *MUC4*) was assessed in different age groups. Compared to the levels in young age group (aged 20–29 years), expression of *MUC3A* and *MUC4* tended to decrease with age, which was prominent in elderly groups (aged 60–79 years) (Fig. 2B and C, respectively). Moreover, expressions of barrier-associated molecules (*MUC3A* and *CLDN3*) were down-regulated in high PKR or high ZAK subjects (Fig. 2C–F), verifying the inverse correlations between ribosomal stress and barrier integrity. From human dataset-based evaluation, it was hypothesized that gut stress-induced barrier disruption may be a crucial cause of reduced longevity in aged organisms. The mechanism of ribosomal stress-associated regulation of the lifespan was investigated further in nematode guts. Morphologically, the ribosomal insult caused a reduction in the number of intestinal nuclei in the gut luminal lining (Fig. 3A and B). Furthermore, *Sek-1* and *Pmk-1* mutants exhibited a more reduction in the number of intestinal nuclei than that in wild-type animals, which was gradually aggravated with time (day 5 and day 12) (Fig. 3A and B). Barrier integrity was tested using a non-absorbable blue food dye and was microscopically visualized. While the majority of staining was observed within the intact gut lumen, ribosomal stress led to partial spreading of the dye into their body cavity (Fig. 3C and D). In contrast, *Sek-1* and *Pmk-1* mutants experienced severe leakage of the dye into the body cavity in response to the ribosomal stress as the exposure time increases. Moreover, *Sek-1* mutants displayed an extensive spread of the luminal contents in the body cavity via severe loss of the gut epithelial barrier integrity in response to DON at day 12. The relative permeability of the gut barrier was monitored by staining the fat under the intestinal epithelial layer using Nile red as a lipophilic fluorescent dye after epithelial barrier disruption (Oil red O was used to counterstain major lipid storage region in the nematodes, Supplementary Figs. 1A–1B). After 24 h exposure to chemical ribosomal stressor, permeability (relative ratio of Nile red/Oil red O) was confirmed, and there was a notable increase in gut permeability in sek-1 deficient animals in response to the ribosomal insult. Moreover, cross-sectional observation of the nematode gut barrier under an electron microscope demonstrated that Sek-1 deficiency led to disruption of the gut epithelial layer in response to the ribosomal insult, although there were rare histological injuries in the horizontal gut epithelial layer of wild-type animals in response to the ribosomal insult in the early age (day 2) (Supplementary Fig. 1C). All of these evidences support the barrier-protective action of Sek-1/Pmk-1-linked signaling in response to the ribosomal insult.

Consistent with the results in the nematode, comparative analysis in the murine model showed a similar pattern of gut barrier regulation. Aging-associated reduction of Sek-1-linked signaling was confirmed in the mouse intestine. In addition to the basal levels of p38 phosphorylation, levels of ribosomal stress-activated p38 MAPK were also attenuated in the guts of old mice (Fig. 4A and B). Functionally, aging-associated barrier responses were evaluated by measuring serum levels of luminally applied fluorescein isothiocyanate [FITC]-dextran in the mice (Fig. 4C). As in the nematode model, the ribosomal insult increased serum FITC-dextran in the mouse gut. Stress-induced barrier disruption was notably aggravated in the elderly subjects compared to the young group. In addition to the epithelial barrier, the mucosal layer and mucin secretions were impaired by the ribosomal insult in mouse gut lumen (Fig. 4D). Compared to young mouse guts, old mouse intestines exhibited similar levels of mucus secretion and goblet cells; however, mucus secretion and number of goblet cells in response to ribosomal stress were severely attenuated in the old animal group, indicating age-associated aggravation of barrier responses to gut insult (Fig. 4E and F). We further mechanistically evaluated the roles of the Sek-1/p38 MAPK signaling pathway in maintaining gut barrier integrity in response to mucosal insult using a porcine enterocyte monolayer

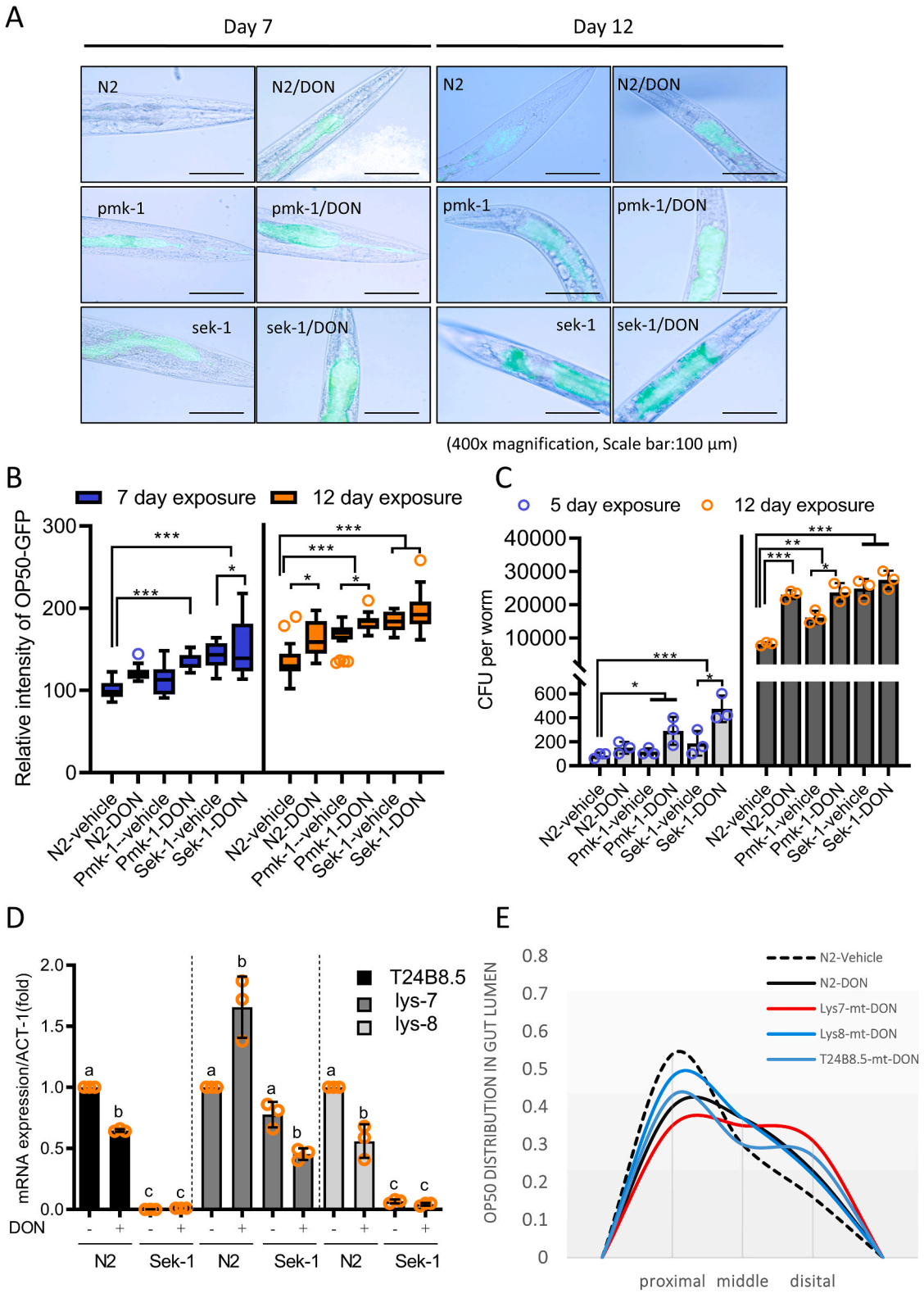

Fig. 5. Ribosomal insult changes gut bacteria colonization in *C. elegans*

A-B. Fluorescence microscopy observation of N2, *Sek-1*, *Pmk-1* mutant nematodes feeding on GFP-expressing *E. coli* OP50 containing vehicle or chemical ribosomal stressor (500 ng/ml DON) for 24 h (left panel) (× 100; scale bar(s), 100 μm) (A). Relative density of GFP-labeled *E. coli* OP50 the gut lining (B). Results are shown as a plot with Tukey whiskers. All data represent three independent experiments (*$p < 0.05$, **$p < 0.01$). **C.** Number of viable intestinal *E. coli* OP50 after exposure of N2, *Sek-1*, *Pmk-1* mutant nematodes in response to vehicle or chemical ribosomal stressor (500 ng/ml DON) for 24 h. Data represent mean ± SD (N = 3) and results are shown as mean values ± SD. Asterisks (*) indicate significant differences between groups (*p < 0.05, ***p < 0.001). **D.** mRNA levels of T24B8.5, *lys-7*, and *lys-8* worms exposed to vehicle or chemical ribosomal stressor (500 ng/ml of DON) for 48 h determined using qPCR. Data represent three independent experiments. Different letters represent significant differences between groups ($p < 0.05$). **E.** Longitudinal distribution of OP50 in the guts of nematodes exposed to vehicle or chemical ribosomal stressor (500 ng/ml of DON) for 48 h. Data represent three independent experiments.

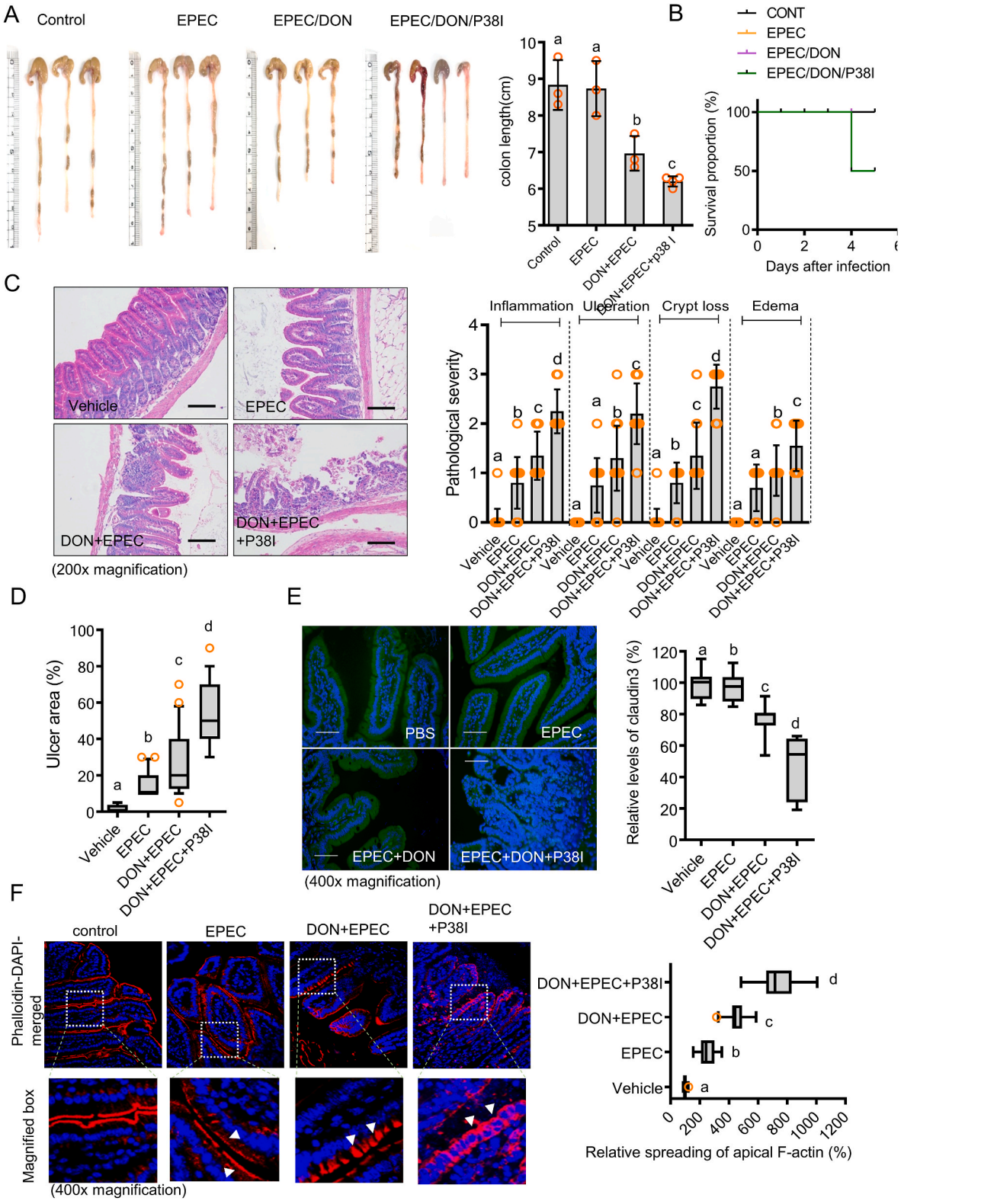

(caption on next page)

Fig. 6. Ribosomal insult exacerbates colitis and barrier disruption in a p38-dependent manner
Mice pretreated with p38 inhibitor (P38I, SB203580, 10 mg/kg, I.P.) for 2 h were exposed to vehicle or chemical ribosomal stressor (25 mg/kg DON) via gavage for 24 h then were orally infected with sterile LB broth or EPEC (1×10^9 CFU) for 4 days (N = 13). **A.** After treatment, colon lengths were compared between groups and were quantified (the right graph). Results are shown as mean values ± SD. Different letters over each bar represent significant differences between groups ($p < 0.05$). **B.** Survival proportion of exposed mice. **C.** Representative histologic observations of hematoxylin and eosin (H&E)-stained small intestine sections by microscopy (left panels) and pathological severity (right graphs) (× 200; scale bar(s), 100 μm). Different letters over each bar represent significant differences between groups ($p < 0.05$). **D.** Extent of ulcerated areas in H&E-stained small intestine samples. Results are shown as a plot with Tukey whiskers. Different letters over each box represent significant differences between groups ($p < 0.05$). **E.** Images of claudin 3 (green) expression in the small intestine and the relative expression (%) of claudin 3 in tissue samples counterstained with DAPI (× 400; scale bar(s), 50 μm). The right graph: quantification of claudin-3 in tissue samples. Results are shown as a plot with Tukey whiskers. Different letters over each box represent significant differences between groups ($p < 0.05$). **F.** F-actin (red) staining and DAPI nuclear staining (blue). White arrows indicate the altered localization of F-actin from apical distribution (left panel) and relative spreading of apical F-actin (%) (the right graph) (× 400; scale bar (s), 50 μm). Results are shown as a plot with Tukey whiskers. Different letters over each box represent significant differences between groups ($p < 0.05$). (For interpretation of the references to color in this figure legend, the reader is referred to the Web version of this article.)

culture. The ribosomal insult led to a reduction in transepithelial electrical resistance (TEER) in monolayer cultures of porcine enterocytes (IPEC-1), which was exacerbated by the blocking of the Sek-1/p38 MAPK signaling pathway (Fig. 4G). Moreover, measurements of intestinal monolayer permeability using FITC-dextran confirmed the deterioration of barrier integrity via the inhibition of p38 MAPK signaling in response to the ribosomal insult (Fig. 4H). Together, these data demonstrate the pivotal function of epithelial p38 MAPK in preventing gut barrier disruption in response to ribosomal insult. The old animals displayed low levels of p38 signaling, thus indicating their high sensitivities to ribosomal stress-induced gut barrier disruption.

3.3. Ribosomal insult increases bacterial exposure in the nematode gut

The maintenance of gut barrier integrity is crucial for the control of microbial colonization during aging. Distribution of gut bacteria was monitored using GFP-labeled OP50. GFP-labeled microbes were quantified in the gut lining, from the mouth to the anus (Fig. 5A–B). At the early age of day 2, gut bacterial levels were too marginal to detect. However, bacterial colonization increased with time of the aging, which was notable under the ribosomal stress at day 12. Moreover, *Sek-1* and *Pmk-1* mutants displayed significantly increased levels of bacterial colonization. In particular, *Sek-1* and *Pmk-1* mutants demonstrated increased transverse migration from the gut lumen to the inner body cavity in response to ribosomal insult relative to that in wild-type nematodes. Moreover, the quantitation of the gut bacteria verified the microscopic observation of bacterial colonization and translocation (Fig. 5C). The ribosomal stress increased the number of intestinal *E. coli.* More bacteria were detected in *Sek-1* and *Pmk-1* mutants than in the wild type animals, indicating the preventive roles of Sek-1/p38 MAPK-associated signaling against bacterial access and colonization in this nematode gut model.

In response to bacterial access, *C. elegans* has evolved its defense against microbial exposure by producing lysozymes in addition to the epithelial barrier junction. In response to ribosomal stress, the animals suppress the production of lysozymes, other than lysozyme 7; however, *Sek-1* mutants displayed attenuated induction of lysozymes, indicating the positive regulation of lysozyme expression by Sek-1 signaling (Fig. 5D). Moreover, GFP-labeled OP50 was quantified in the three segments of the gut lining, from the mouth to the anus during longitudinal observation. Lysozyme-mutant animals were more susceptible to longitudinal translocation of the gut bacteria at the distal section of the gut in response to the ribosomal insult (Fig. 5E). Taken together, Sek-1 signaling was found to be important in microbial regulation of the nematode gut in response to the ribosomal stress via lysozyme production and enhanced integrity of the mucosa and epithelial lining.

3.4. Disruption of the murine intestinal barrier allows greater microbial access

Consistent with the results from the nematode gut model, ribosomal insult increased susceptibility to luminal bacterial translocation in the murine model. Enteropathogenic *E. coli* (EPEC) is a human enteric pathogen that attaches to the surface of intestinal epithelial cells and causes watery diarrhea; however, in mice, EPEC infections result in relatively mild symptoms, such as histological changes (e.g., increased numbers of lamina propria neutrophils) without diarrhea [57]. In the present study, EPEC infection did not cause diarrhea or intestinal shortening in the murine model (Fig. 6A); however, EPEC infection shortened colon length in ribosome-insulted animals, which was much more severe when p38 MAPK was inhibited. Moreover, inhibition of p38 MAPK increased mouse mortality, implicating p38 MAPK-dependent resistance to EPEC infection (Fig. 6B). Similarly, the length of the intestinal villi was shortened in response to EPEC infection, and this phenomenon was particularly prominent in ribosome-insulted hosts in a p38 MAPK-associated manner (Supplementary Fig. 1D). In terms of pathological scoring, the ribosomal insult aggravated infection-linked disease severity in the gut. Moreover, p38 inhibition in the EPEC-infected gut with pre-exposure to the ribosomal stress resulted in severe epithelial loss, ulceration, and inflammatory lesions (Fig. 6C and D). Intestinal epithelial loss was further confirmed by the measurement of claudin 3 expression as a representative junctional molecule in response to the ribosomal insult. Epithelial claudin 3 was similarly regulated in the murine infection model. The ribosomal insult reduced the expression of claudin 3, which was severely reduced in host guts where p38 MAPK was inhibited during EPEC infection (Fig. 6E). F-actin is strongly localized to the apical surface of the epithelium, while the ribosomal insult exacerbated the disruption of this marker of epithelial polarity in response to EPEC infection, triggering the spread of F-actin to basolateral regions (Fig. 6F). Furthermore, the inhibition of p38 MAPK led to a complete loss of polarity and even distribution of F-actin throughout the epithelial cells, indicating the regulatory role of p38-linked signaling in the maintenance of enterocyte polarity in response to the ribosomal insult.

In addition to influences on the epithelial barrier, the mucosal barrier was assessed by evaluating mucus secretion by the gut epithelia. EPEC infection led to a slight decrease in mucus secretion, which was exacerbated by the ribosomal stress (Fig. 7A). Of note, p38 inhibition completely depleted mucus production in the guts of mice infected with EPEC after ribosomal insult. Along with a reduction in mucin production, secretion of the antibacterial peptides such as lysozymes demonstrated similar patterns in the murine model. The ribosomal insult significantly downregulated lysozyme expression in the guts of mice infected with EPEC, while p38 MAPK positively regulated lysozyme secretion in response to EPEC infection (Fig. 7B). The insult disrupted the mucosal barriers (mucus and lysozyme secretion) between luminal bacteria and epithelia, which are crucial for defense against luminal bacteria. Barrier disruption led to increased accessibility of the gut bacteria (Fig. 7C) and EPEC (Fig. 7D) to the gut epithelial layer. Moreover, p38 inhibition in EPEC-infected guts displayed complete loss of the mucosal barrier and subsequent access of luminal commensal and pathogenic bacteria toward the epithelial layer under the ribosomal insult (Fig. 7C and D), indicating a protective role of the p38 pathway against gut microbiota and enteric pathogens, consistent with findings in

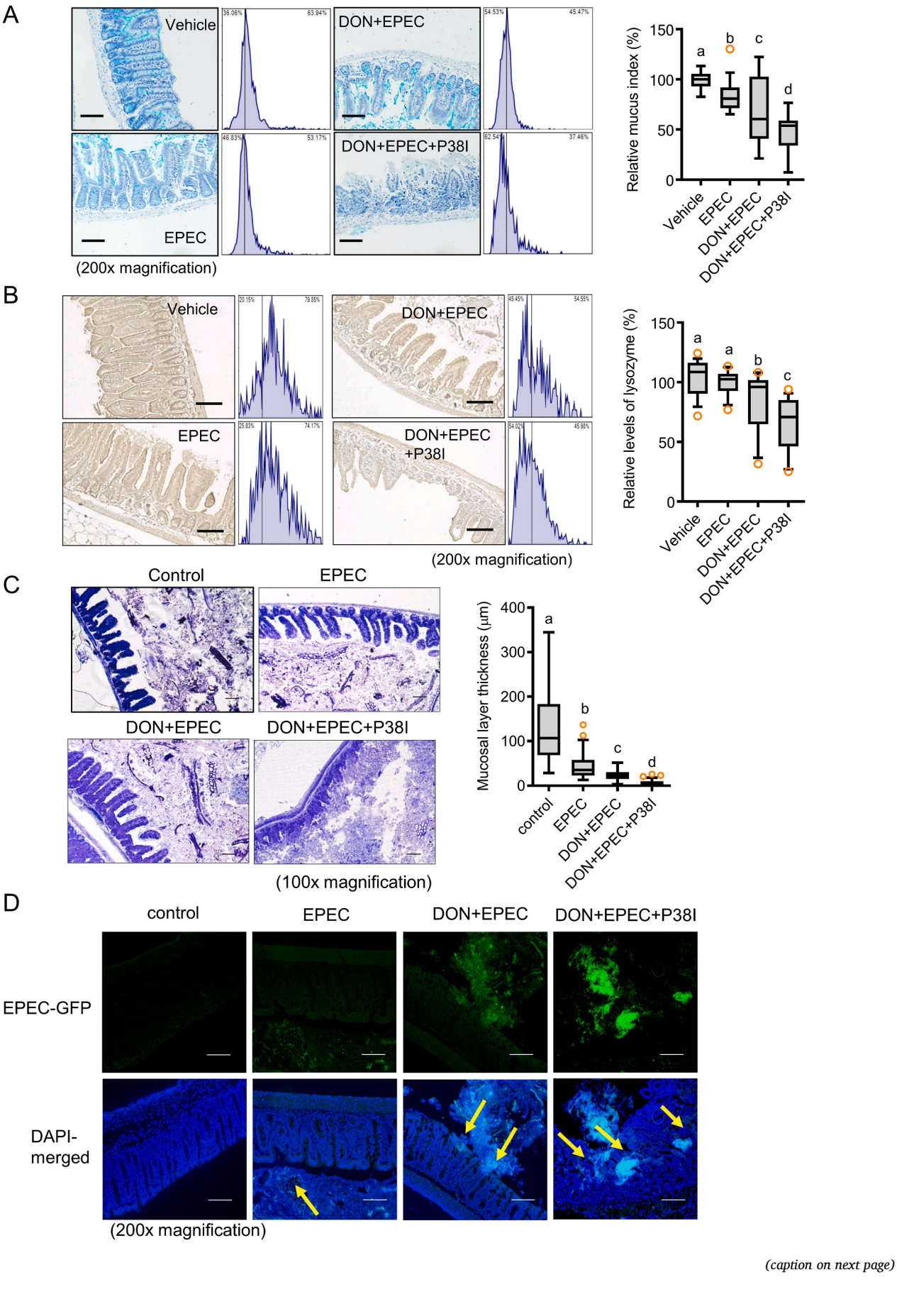

(caption on next page)

Fig. 7. Ribosomal insult exacerbates EPEC infection via gut barrier disruption in a p38-dependent manner
Mice pretreated with p38 inhibitor (P38I, SB203580, 10 mg/kg, I.P.) for 2 h were exposed to vehicle or chemical ribosomal stressor (25 mg/kg DON) via gavage for 24 h then orally infected with sterile LB broth or EPEC (1×10^9 CFU) for 4 days (N = 13). **A.** Lysozyme expression in the small intestine with hematoxylin counterstaining (× 200; scale bar(s), 100 μm). The relative lysozyme density was measured using Histoquest analysis software. Relative quantitation is shown as a plot with Tukey whiskers. Different letters over each box represent significant differences between groups ($p < 0.05$). **B.** Mucin secretion in small intestines (alcian blue, positive) (× 200; scale bar(s), 100 μm). Right panel: mucus indices for images to the left. Relative quantitation is shown as a plot with Tukey whiskers. Different letters over each box represent significant differences between groups ($p < 0.05$). **C.** Gram staining to determine the ability of total bacteria to access the epithelial barrier (× 100; scale bar(s), 100 μm). Relative quantitation of the mucosal thickness is shown as a plot with Tukey whiskers (the right graph). Different letters over each box represent significant differences between groups ($p < 0.05$). **D.** Measurement of GFP-labeled EPEC in the mucus to determine its ability to access gut epithelia, counterstained with DAPI (× 200; scale bar(s), 100 μm). (For interpretation of the references to color in this figure legend, the reader is referred to the Web version of this article.)

the nematode model (Fig. 5). Taken together, our data indicate that ribosomal insult disrupts the integrity of both the epithelial and mucosal barrier in a p38 MAPK-dependent manner, which may account for the increased invasion of commensal and pathogenic bacteria in the murine model.

3.5. Ribosomal stress-responsive microbiota predicts the mucin degradation in the aged animals

In addition to stress-induced barrier disruption during the aging, we evaluated the effects of the chemical ribosomal stressor (DON) on the microbial community in the aged subjects. Since DON specifically binds to the eukaryotic ribosomes, the potent effect of DON on the bacterial community would be due to alterations in host pathophysiological states rather than a direct impact on the microbes. The alpha diversity based on the Shannon metrics showed that the microbial communities under the ribosomal stress had a lower degree of diversity than those in the aged control mice (Supplementary Fig. 2A). Moreover, the ribosomal insult caused pronounced changes in gut microbiota composition, such as an increased proportion of Phylum Bacteroidota with a decrease in Phylum Firmicutes (Supplementary Fig. 2B). Furthermore, the decrease in Firmicutes was due to reduction in Class Clostridia population whereas the increase in Phylum Bacteroidota was linked to the reduced population of bacteroidia in response to chemical ribosomal insult (Supplementary Fig. 2C). Closer observation of high abundant genus or species demonstrated that the abundance of *Muribaculum* and *Duncaniella dubosii* were notably elevated by the ribosomal stress (Fig. 8A). In terms of mucosal barrier disruption, members of the underexplored family Muribaculaceae were recently revealed as major mucin monosaccharide foragers [58]. In the present study, the concomitant increase in Muribaculaceae members such as *Muribaculum* and *Duncaniella dubosii* predicts the disruption of the mucosal layer over the epithelial lining in response to the ribosomal stress and altered bacterial community. Furthermore, the metagenomic prediction based on the 16S rRNA profile using *PICRUSt2* demonstrated significant elevations in genes encoding mucin degradation-related enzymes in response to ribosomal stress in the aged mice (Fig. 8B). In particular, genes for beta-galactosidase (EC:3.2.1.23), alpha-L-fucosidase (EC:3.2.1.51), beta-N-acetylhexosaminidase (EC:3.2.1.52), alpha-galactosidase (EC:3.2.1.22), alpha-glucosidase (EC:3.2.1.20), sialate O-acetylesterase (EC:3.1.1.53), exo-alpha-sialidase (EC:3.2.1.18), beta-mannosidase (EC:3.2.1.25), and alpha-N-acetylglucosaminidase (EC:3.2.1.50) were significantly enhanced by the chemical ribosomal stress in the aged mice. Taken together, the abundances in mucin metabolism-linked bacteria and enzymes were concomitantly increased with the mucosal barrier disruption by the ribosomal stress with aging.

4. Discussion

In response to internal or external insults, the ribosomes are crucial in managing the cellular integrity. Since levels of biomarkers for the ribosomal stress and dysfunction are elevated with aging in humans, we simulated the actions of the ribosomal dysfunction in the aging process using a most frequently-exposed ribosome-targeting agent in human environment. DON is the most frequently occurring ribotoxic stressor primarily produced by *Fusarium species* [59,60]. The molds colonize more than 60–70% of global agricultural commodities, including a variety of cereal-based foodstuffs and animal feed [4,5]. In addition to contaminating crops, DON is released into surface soil water and drainage systems and is a micropollutant in soil and aqueous environments [6–8]. The aged hosts exhibit greater susceptibility to DON-induced disruption of the epithelial and mucosal barriers of the gut than that by young animals, which was concomitant with attenuation of Sek-1/p38-associated signaling during aging process. Since Sek-1 is positively involved in the maintenance of junctional molecules and the expression of antimicrobial lysozymes, its signaling attenuation in the aged subjects may account for their increased susceptibility to barrier disruption and subsequent microbial access. Moreover, the abundances in mucosa-foraging bacteria and genes for mucin metabolism-linked enzymes were elevated with the mucosal barrier disruption in the ribosome-insulted aged subjects (Fig. 8C). For longevity, it is crucial to maintain barrier-associated defenses against microbial access. A weakened gut lining in aged hosts may allow exogenous or indigenous microbes to translocate through the barrier and evoke inflammatory responses, leading to sepsis and mortality, although the microbes themselves are hardly pathogenic. During the aging process, ribosomal stress-activated Sek-1/p38 MAPK-associated signals are considered beneficial for the defense against mucosal access and in counteracting gastrointestinal insult, including the barrier disruption. These endogenous defense signals diminish during aging and may exacerbate gut toxicity and disease susceptibility with dysbiotic bacterial community in elderly hosts. We have no direct evidence that the ribosomal insult directly reduces human life expectancy; however, the ribosomal stress-associated molecular features are elevated with aging process, which is closely associated with increased disruption of gut barrier integrity. Deleterious effects of aging-associated ribosomal insult on gut barrier integrity may contribute to increased susceptibility to life-threatening microbial and inflammatory risks in a Sek-1/p38-inversed way, which function similarly in both worm and mouse models. Considering molecular and cellular pathways, there is a notably high level of conservation between *C. elegans* and mammals including humans. Among the available 18,452 *C. elegans* protein sequences, at least 83% (15,344 sequences) of worm proteome has human homologous genes [61]. Moreover, worms present evolutionary conserved signaling pathways including the Ras, the Wnt, the Smad, and the Notch pathway as well as MAPK-associated signals, which are involved in complex human diseases or biological processes such as aging. Toxicological consistency between worms and mammals in the present study suggests a usefulness of the worm exposure model to elucidate the causal effects of environmental and human health risk factors in a one health perspective (Fig. 8C).

Among aging-associated molecular mechanisms, alterations of the translation machinery of the ribosomes can be a central module of the protein homeostasis during the aging process [62]. Excessive protein biosynthesis can lead to accumulation of erroneous malfunctional proteins which are potently toxic to cellar integrity during aging. The disturbance in protein homeostasis can be minimized by global translational arrest via depletion of components of the translational

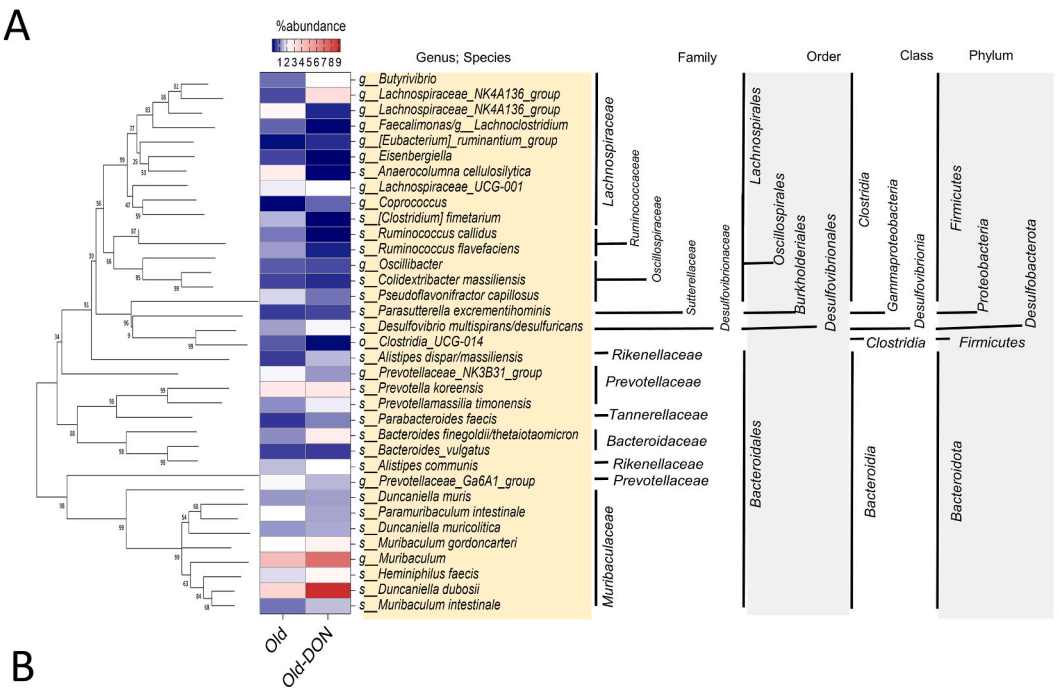

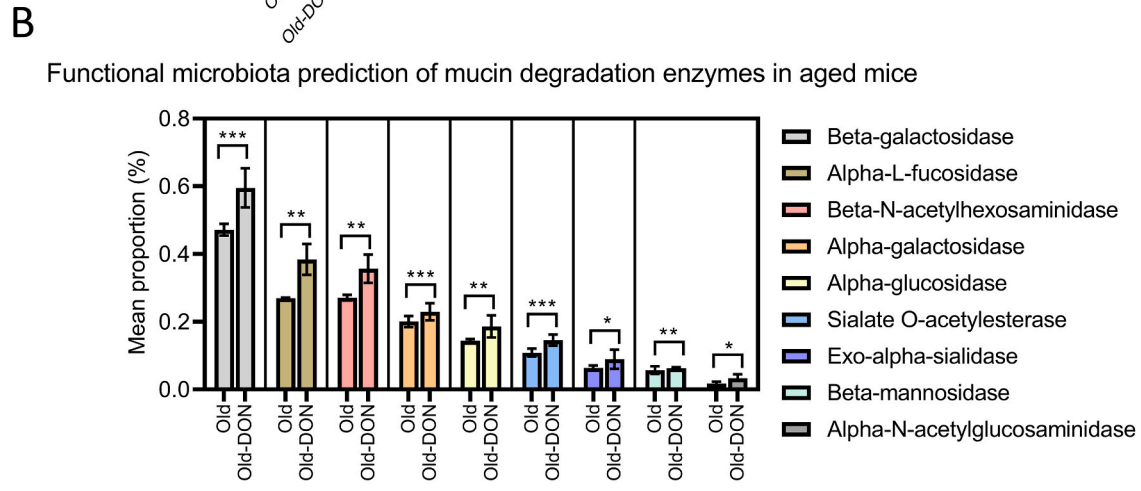

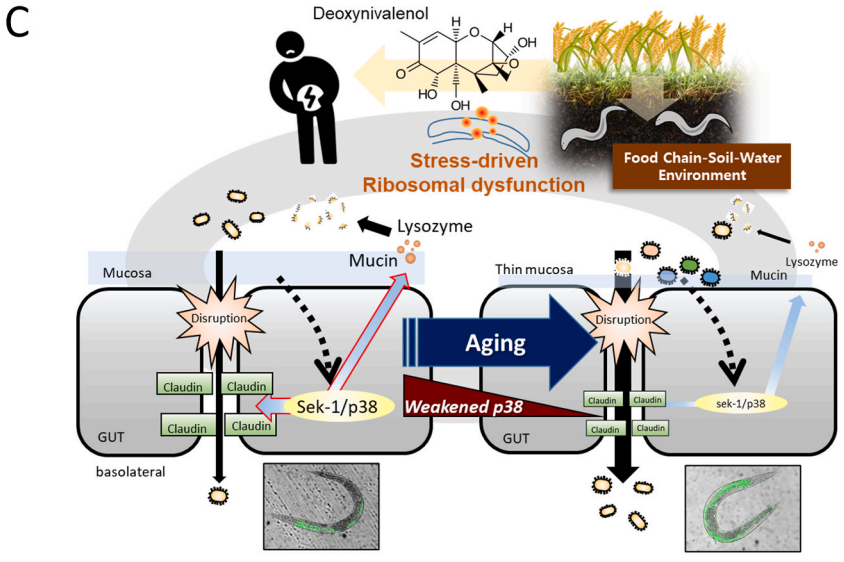

(caption on next page)

Fig. 8. Ribosomal stress alters bacterial community in the aged mice
A-B. Nineteen-month-old male mice were exposed to chemical ribosomal stressor (25 mg DON/kg body weight) via gavage for 12 h (N = 20), and stools were collected after the exposure. The fecal bacterial DNA was subjected to 16S rRNA analysis for the determination of the phylogenetic composition. **A**. The bacteria of each top 30 abundant taxa are listed along with the corresponding abundance in aged mice exposed to the vehicle or DON. **B**. Bacterial genes related to mucin degradation enzymes reconstructed from 16S rRNA profile with *PICRUSt2*. Data represent mean ± SD (N = 3) and results are shown as mean values ± SD. Asterisks (*) indicate significant differences between groups (*$p < 0.05$, **$p < 0.01$, ***$p < 0.001$). **C.** A variety of biological systems can be exposed to the ribosomal stressors including a most prevalent mycotoxin deoxynivalenol in the food chain on the planet. As a protective pathway in response to ribosomal stress, Sek-1/p38 MAPK signaling is activated to facilitate the induction of antimicrobial mediators and maintain barrier integrity. However, the aging process attenuates Sek-1/p38 signaling activation in the gut, thus, barrier defense is weakened due to reduced protective signaling, leading to increased insult by mucosa-degrading gut microbes with aging. Overall, the ribosomal insult-related gut deterioration is aggravated with aging, ultimately increasing infection-linked risk in a p38-dependent manner.

machinery [63]. Therefore, longevity can be associated with the attenuation of the global protein synthesis. However, some proteins are needed to be upregulated for damage repair and cellular maintenance during aging process. This selective upregulation of the protective proteins can be facilitated by stress-responsive signaling modules during the aging process. In the present study, we focused on ribosomal stress-activated Sek-1/p38 signaling as the protective platform in the epithelial cell integrity. p38 MAPK is an evolutionarily conserved MAPK subfamily that has four isoforms, α, β, δ, and γ. It can act as a direct sentinel for various stress factors, including oxidative stress, inflammatory cytokines and growth factors, and organelle-associated stress [1,2,64]. In response to external and internal insults, cells undergo reprograming processes associated with proliferation, differentiation, and cell death in response to cues from tissues or circulating factors, including growth factors, hormones, and cytokines, which leads to the activation of MAPK [1]. In particular, when ribosomal insults are recognized by the ribosomal scaffold, p38 MAPK signal transduction pathways are activated in human and murine cells [1,2]. In the present study, Sek-1/p38 MAPK signaling protected both mammalian and *C. elegans* model animals against aging-associated gut damage, whereas Sek-1/p38 MAPK signaling-mediated benefits were attenuated by the aging process. Aging is associated with a decline in the activity of the conserved p38 MAPK signaling pathway, which weakens innate immunity against luminal bacteria [65]. Among the downstream transcription factors in *C. elegans*, activating transcription factor 7 (ATF7), an ortholog of mammalian ATF2/ATF7, mediates the regulation of genes involved in innate immunity, including C-type lectins, ShK toxins, and CUB-like genes [66,67]. In addition to its involvement in antimicrobial gene induction, Sek-1/p38 MAPK signaling contributes to prolonging animal lifespan through the regulation of oxidative stress responses [68]. Specifically, p38 MAPK mediates the activity of the oxidative stress-induced Cap-N-Collar transcription factor, SKN-1. In response to oxidative stress, enterocytes exhibit nuclear accumulation of the SKN-1 protein, leading to the induction of a phase II detoxification enzyme involved in the maintenance of gut barrier integrity [68]. The p38 MAPK-mediated regulation of oxidative stress has also been confirmed in a mammalian model [69]; therefore, diminished p38 MAPK signaling transduction in the aged host may aggravate oxidative injuries in the gut, while the production of antimicrobial mediators is reduced, allowing increased microbial invasion in the body.

5. Conclusion

Based on the genetic features of aging-associated ribosomal dysfunction in humans, we simulated the actions of the ribosomal stress in the aging process using DON, a ribosome-targeting xenobiotic agent. The aged hosts exhibit greater susceptibility to ribosomal stress-induced disruption of the epithelial and mucosal barriers of the gut than that by young subjects, which was concomitant with attenuation of Sek-1/p38-associated signaling during the aging process. Since Sek-1/p38-associated signaling is positively involved in the maintenance of junctional and antimicrobial molecules, aging-associated attenuation of the protective signaling accounts for the increased barrier distress and susceptibility to dysbiotic community including muco-foragers in the aged hosts. In order to provide translational interventions against ribosomal stress-linked gut aging, a systematic network of the chronic adverse outcome pathway needs to be carefully addressed in the future investigations.

Funding

This research was supported by the Basic Science Research Program through the National Research Foundation of Korea (NRF), funded by the Ministry of Education (2018R1D1A3B05041889).

CRediT authors contribution statement

Junjie Sun: investigation and formal analysis of the worm model. Juil Kim: investigation and formal analysis of mammalian models. Hoyoung Jeong: bacterial bioinformatic analysis. Dasom Kwon: fecal sample analysis and validation. Yuseok Moon: supervision, conceptualization, methodology, formal analysis, visualization, writing - original draft, and writing - review & editing.

Declaration of competing interest

The authors declare that they have no known competing financial interests or personal relationships that could have influenced the work reported in this paper.

Data availability

Data will be made available on request.

Acknowledgements

We greatly appreciate for the technical assistance and protocols for worm and murine experiments by Jiyeon Park and Mira Yu.

Appendix A. Supplementary data

Supplementary data to this article can be found online at https://doi.org/10.1016/j.redox.2022.102565.

References

[1] J.D. Laskin, D.E. Heck, D.L. Laskin, The ribotoxic stress response as a potential mechanism for MAP kinase activation in xenobiotic toxicity, Toxicol. Sci. : Off. J. Soc. Toxicol. 69 (2002) 289–291.
[2] V.I. Shifrin, P. Anderson, Trichothecene mycotoxins trigger a ribotoxic stress response that activates c-Jun N-terminal kinase and p38 mitogen-activated protein kinase and induces apoptosis, J. Biol. Chem. 274 (1999) 13985–13992.
[3] S.H. Park, et al., Repression of peroxisome proliferator-activated receptor gamma by mucosal ribotoxic insult-activated CCAAT/enhancer-binding protein homologous protein, J. Immunol. 185 (2010) 5522–5530, https://doi.org/10.4049/jimmunol.1001315.
[4] M.C. Smith, S. Madec, E. Coton, N. Hymery, Natural Co-occurrence of mycotoxins in foods and feeds and their in vitro combined toxicological effects, Toxins 8 (2016) 94, https://doi.org/10.3390/toxins8040094.
[5] H.J. Lee, D. Ryu, Worldwide occurrence of mycotoxins in cereals and cereal-derived food products: public health perspectives of their Co-occurrence, J. Agric. Food Chem. 65 (2017) 7034–7051, https://doi.org/10.1021/acs.jafc.6b04847.

[6] J. Schenzel, R.P. Schwarzenbach, T.D. Bucheli, Multi-residue screening method to quantify mycotoxins in aqueous environmental samples, J. Agric. Food Chem. 58 (2010) 11207–11217, https://doi.org/10.1021/jf102737q.

[7] J. Schenzel, K. Hungerbuhler, T.D. Bucheli, Mycotoxins in the environment: II. Occurrence and origin in Swiss river waters, Environ. Sci. Technol. 46 (2012) 13076–13084, https://doi.org/10.1021/es301558v.

[8] L.M. Juraschek, A. Kappenberg, W. Amelung, Mycotoxins in soil and environment, Sci. Total Environ. 814 (2022), 152425, https://doi.org/10.1016/j.scitotenv.2021.152425.

[9] M.S. Iordanov, et al., Ribotoxic stress response: activation of the stress-activated protein kinase JNK1 by inhibitors of the peptidyl transferase reaction and by sequence-specific RNA damage to the alpha-sarcin/ricin loop in the 28S rRNA, Mol. Cell Biol. 17 (1997) 3373–3381.

[10] M.S. Iordanov, et al., Ultraviolet radiation triggers the ribotoxic stress response in mammalian cells, J. Biol. Chem. 273 (1998) 15794–15803.

[11] M. Li, J.J. Pestka, Comparative induction of 28S ribosomal RNA cleavage by ricin and the trichothecenes deoxynivalenol and T-2 toxin in the macrophage, Toxicol. Sci. : Off. J. Soc. Toxicol. 105 (2008) 67–78, https://doi.org/10.1093/toxsci/kfn111.

[12] T. Girbes, J.M. Ferreras, F.J. Arias, F. Stirpe, Description, distribution, activity and phylogenetic relationship of ribosome-inactivating proteins in plants, fungi and bacteria, Mini Rev. Med. Chem. 4 (2004) 461–476.

[13] J. Lacadena, et al., Fungal ribotoxins: molecular dissection of a family of natural killers, FEMS Microbiol. Rev. 31 (2007) 212–237.

[14] T.B. Ng, J.H. Wong, H. Wang, Recent progress in research on ribosome inactivating proteins, Curr. Protein Pept. Sci. 11 (2010) 37–53.

[15] F. Stirpe, M.G. Battelli, Ribosome-inactivating proteins: progress and problems, Cell. Mol. Life Sci. 63 (2006) 1850–1866.

[16] H. Bae, et al., Hematopoietic cell kinase associates with the 40S ribosomal subunit and mediates the ribotoxic stress response to deoxynivalenol in mononuclear phagocytes, Toxicol. Sci. : Off. J. Soc. Toxicol. 115 (2010) 444–452, https://doi.org/10.1093/toxsci/kfq055.

[17] Z. Du, K.H. Kim, J. Kim, Y. Moon, Fungal deoxynivalenol-induced enterocyte distress is attenuated by adulterated adlay: in vitro evidences for mucoactive counteraction, Front. Immunol. 9 (2018) 186, https://doi.org/10.3389/fimmu.2018.00186.

[18] J.S. Gray, H.K. Bae, J.C. Li, A.S. Lau, J.J. Pestka, Double-stranded RNA-activated protein kinase mediates induction of interleukin-8 expression by deoxynivalenol, Shiga toxin 1, and ricin in monocytes, Toxicol. Sci. 105 (2008) 322–330.

[19] H.R. Zhou, A.S. Lau, J.J. Pestka, Role of double-stranded RNA-activated protein kinase R (PKR) in deoxynivalenol-induced ribotoxic stress response, Toxicol. Sci. 74 (2003) 335–344.

[20] S. Mishra, et al., Deoxynivalenol induced mouse skin tumor initiation: elucidation of molecular mechanisms in human HaCaT keratinocytes, Int. J. Cancer 139 (2016) 2033–2046, https://doi.org/10.1002/ijc.30260.

[21] F. Graziani, et al., The food-associated ribotoxin deoxynivalenol modulates inducible NO synthase in human intestinal cell model, Toxicol. Sci. 145 (2015) 372–382, https://doi.org/10.1093/toxsci/kfv058.

[22] J.M. Yoder, R.U. Aslam, N.J. Mantis, Evidence for widespread epithelial damage and coincident production of monocyte chemotactic protein 1 in a murine model of intestinal ricin intoxication, Infect. Immun. 75 (2007) 1745–1750.

[23] K.H. Kim, S.J. Lee, J. Kim, Y. Moon, Dynamic malignant wave of ribosome-insulted gut niche via the Wnt-CTGF/CCN2 circuit, iScience 23 (2020), 101076, https://doi.org/10.1016/j.isci.2020.101076.

[24] S.H. Park, J. Kim, Y. Moon, Caveolar communication with xenobiotic-stalled ribosomes compromises gut barrier integrity, Commun. Biol. 3 (2020) 270, https://doi.org/10.1038/s42003-020-0994-1.

[25] D. Payros, et al., The food contaminant, deoxynivalenol, modulates the Thelper/Treg balance and increases inflammatory bowel diseases, Arch. Toxicol. (2020), https://doi.org/10.1007/s00204-020-02817-z.

[26] Y. Luo, T. Yoshizawa, T. Katayama, Comparative study on the natural occurrence of Fusarium mycotoxins (trichothecenes and zearalenone) in corn and wheat from high- and low-risk areas for human esophageal cancer in China, Appl. Environ. Microbiol. 56 (1990) 3723–3726.

[27] F.Q. Li, Y.W. Li, X.Y. Luo, T. Yoshizawa, Fusarium toxins in wheat from an area in Henan Province, PR China, with a previous human red mould intoxication episode, Food Addit. Contam. 19 (2002) 163–167.

[28] R.V. Bhat, S.R. Beedu, Y. Ramakrishna, K.L. Munshi, Outbreak of trichothecene mycotoxicosis associated with consumption of mould-damaged wheat production in Kashmir Valley, India, Lancet 1 (1989) 35–37.

[29] L. Tran, B. Greenwood-Van Meerveld, Age-associated remodeling of the intestinal epithelial barrier, J. Gerontol. A. Biol. Sci. Med. Sci. 68 (2013) 1045–1056, https://doi.org/10.1093/gerona/glt106.

[30] R. Pukkila-Worley, F.M. Ausubel, Immune defense mechanisms in the Caenorhabditis elegans intestinal epithelium, Curr. Opin. Immunol. 24 (2012) 3–9, https://doi.org/10.1016/j.coi.2011.10.004.

[31] A. Tong, et al., Negative regulation of Caenorhabditis elegans epidermal damage responses by death-associated protein kinase, Proc. Natl. Acad. Sci. U. S. A 106 (2009) 1457–1461, https://doi.org/10.1073/pnas.0809339106.

[32] Q. Wu, et al., Contributions of altered permeability of intestinal barrier and defecation behavior to toxicity formation from graphene oxide in nematode Caenorhabditis elegans, Nanoscale 5 (2013) 9934–9943, https://doi.org/10.1039/c3nr02084c.

[33] S. Tsukita, M. Furuse, Claudin-based barrier in simple and stratified cellular sheets, Curr. Opin. Cell Biol. 14 (2002) 531–536.

[34] O. Zugasti, et al., Activation of a G protein-coupled receptor by its endogenous ligand triggers the innate immune response of Caenorhabditis elegans, Nat. Immunol. 15 (2014) 833–838, https://doi.org/10.1038/ni.2957.

[35] H.J. An, , et al.A.P.P.A.R. Pan Agonist, MHY2013 alleviates age-related hepatic lipid accumulation by promoting fatty acid oxidation and suppressing inflammation, Biol. Pharm. Bull. 41 (2018) 29–35, https://doi.org/10.1248/bpb.b17-00371.

[36] H.J. Choi, et al., Early epithelial restitution by nonsteroidal anti-inflammatory drug-activated gene 1 counteracts intestinal ulcerative injuries, J. Immunol. 197 (2016) 1415–1424, https://doi.org/10.4049/jimmunol.1501784.

[37] M. Yu, J. Kim, J.H. Ahn, Y. Moon, Nononcogenic restoration of the intestinal barrier by E. coli-delivered human EGF, JCI Insight 4 (2019), https://doi.org/10.1172/jci.insight.125166.

[38] J. Kim, Y. Moon, Worm-based alternate assessment of probiotic intervention against gut barrier infection, Nutrients 11 (2019), https://doi.org/10.3390/nu11092146.

[39] H.J. Choi, J. Kim, K.H. Do, S.H. Park, Y. Moon, Prolonged NF-kappaB activation by a macrophage inhibitory cytokine 1-linked signal in enteropathogenic Escherichia coli-infected epithelial cells, Infect. Immun. 81 (2013) 1860–1869, https://doi.org/10.1128/IAI.00162-13.

[40] S.H. Park, J. Kim, D. Kim, Y. Moon, Mycotoxin detoxifiers attenuate deoxynivalenol-induced pro-inflammatory barrier insult in porcine enterocytes as an in vitro evaluation model of feed mycotoxin reduction, Toxicol. Vitro 38 (2017) 108–116, https://doi.org/10.1016/j.tiv.2016.10.003.

[41] S. Bouhet, et al., The mycotoxin fumonisin B1 alters the proliferation and the barrier function of porcine intestinal epithelial cells, Toxicol. Sci. : Off. J. Soc. Toxicol. 77 (2004) 165–171, https://doi.org/10.1093/toxsci/kfh006.

[42] P. Pinton, et al., Deoxynivalenol impairs porcine intestinal barrier function and decreases the protein expression of claudin-4 through a mitogen-activated protein kinase-dependent mechanism, J. Nutr. 140 (2010) 1956–1962, https://doi.org/10.3945/jn.110.123919.

[43] A.M. Bolger, M. Lohse, B. Usadel, Trimmomatic: a flexible trimmer for Illumina sequence data, Bioinformatics 30 (2014) 2114–2120.

[44] E. Bolyen, et al., Reproducible, interactive, scalable and extensible microbiome data science using QIIME 2, Nat. Biotechnol. 37 (2019) 852–857, https://doi.org/10.1038/s41587-019-0209-9.

[45] B.J. Callahan, et al., DADA2: high-resolution sample inference from Illumina amplicon data, Nat. Methods 13 (2016) 581.

[46] C. Quast, et al., The SILVA ribosomal RNA gene database project: improved data processing and web-based tools, Nucleic Acids Res. 41 (2012) D590–D596.

[47] K. Katoh, K. Misawa, K.i. Kuma, T. Miyata, MAFFT: a novel method for rapid multiple sequence alignment based on fast Fourier transform, Nucleic Acids Res. 30 (2002) 3059–3066.

[48] D. Lane, 16S/23S rRNA sequencing, Nucleic acid Tech. bacterial Syst. (1991) 115–175.

[49] M.N. Price, P.S. Dehal, A.P. Arkin, FastTree 2–approximately maximum-likelihood trees for large alignments, PLoS One 5 (2010), e9490.

[50] G. Stecher, K. Tamura, S. Kumar, Molecular evolutionary genetics analysis (MEGA) for macOS, Mol. Biol. Evol. 37 (2020) 1237–1239, https://doi.org/10.1093/molbev/msz312.

[51] A.C. Vind, et al., ZAKalpha recognizes stalled ribosomes through partially redundant sensor domains, Mol. Cell 78 (2020) 700–713, https://doi.org/10.1016/j.molcel.2020.03.021, e707.

[52] I. Rodrigues, K. Naehrer, A three-year survey on the worldwide occurrence of mycotoxins in feedstuffs and feed, Toxins 4 (2012) 663–675, https://doi.org/10.3390/toxins4090663.

[53] Y. Moon, H. Yang, S.H. Lee, Modulation of early growth response gene 1 and interleukin-8 expression by ribotoxin deoxynivalenol (vomitoxin) via ERK1/2 in human epithelial intestine 407 cells, Biochem. Biophys. Res. Commun. 362 (2007) 256–262.

[54] M.S. Iordanov, B.E. Magun, Loss of cellular K+ mimics ribotoxic stress. Inhibition of protein synthesis and activation of the stress kinases SEK1/MKK4, stress-activated protein kinase/c-Jun NH2-terminal kinase 1, and p38/HOG1 by palytoxin, J. Biol. Chem. 273 (1998) 3528–3534.

[55] W.E. Smith, et al., Shiga toxin 1 triggers a ribotoxic stress response leading to p38 and JNK activation and induction of apoptosis in intestinal epithelial cells, Infect. Immun. 71 (2003) 1497–1504.

[56] J.W. Yu, A. Farias, I. Hwang, T. Fernandes-Alnemri, E.S. Alnemri, Ribotoxic stress through p38 mitogen-activated protein kinase activates in vitro the human pyrin inflammasome, J. Biol. Chem. 288 (2013) 11378–11383, https://doi.org/10.1074/jbc.M112.448795.

[57] S.D. Savkovic, J. Villanueva, J.R. Turner, K.A. Matkowskyj, G. Hecht, Mouse model of enteropathogenic Escherichia coli infection, Infect. Immun. 73 (2005) 1161–1170, https://doi.org/10.1128/IAI.73.2.1161-1170.2005.

[58] F.C. Pereira, et al., Rational design of a microbial consortium of mucosal sugar utilizers reduces Clostridiodes difficile colonization, Nat. Commun. 11 (2020) 5104, https://doi.org/10.1038/s41467-020-18928-1.

[59] M. Kushiro, Effects of milling and cooking processes on the deoxynivalenol content in wheat, Int. J. Mol. Sci. 9 (2008) 2127–2145, https://doi.org/10.3390/ijms9112127.

[60] M. Maresca, J. Fantini, Some food-associated mycotoxins as potential risk factors in humans predisposed to chronic intestinal inflammatory diseases, Toxicon 56 (2010) 282–294.

[61] C.H. Lai, C.Y. Chou, L.Y. Ch'ang, C.S. Liu, W. Lin, Identification of novel human genes evolutionarily conserved in Caenorhabditis elegans by comparative

proteomics, Genome Res. 10 (2000) 703–713, https://doi.org/10.1101/gr.10.5.703.
[62] Y. Gonskikh, N. Polacek, Alterations of the translation apparatus during aging and stress response, Mech. Ageing Dev. 168 (2017) 30–36, https://doi.org/10.1016/j.mad.2017.04.003.
[63] M. Hansen, et al., Lifespan extension by conditions that inhibit translation in Caenorhabditis elegans, Aging Cell 6 (2007) 95–110, https://doi.org/10.1111/j.1474-9726.2006.00267.x.
[64] A. Cuenda, S. Rousseau, p38 MAP-kinases pathway regulation, function and role in human diseases, Biochim. Biophys. Acta 1773 (2007) 1358–1375, https://doi.org/10.1016/j.bbamcr.2007.03.010.
[65] M.J. Youngman, Z.N. Rogers, D.H. Kim, A decline in p38 MAPK signaling underlies immunosenescence in Caenorhabditis elegans, PLoS Genet. 7 (2011), e1002082, https://doi.org/10.1371/journal.pgen.1002082.
[66] R.P. Shivers, et al., Phosphorylation of the conserved transcription factor ATF-7 by PMK-1 p38 MAPK regulates innate immunity in Caenorhabditis elegans, PLoS Genet. 6 (2010), e1000892, https://doi.org/10.1371/journal.pgen.1000892.
[67] E.R. Troemel, et al., p38 MAPK regulates expression of immune response genes and contributes to longevity in C. elegans, PLoS Genet. 2 (2006) e183, https://doi.org/10.1371/journal.pgen.0020183.
[68] H. Inoue, et al., The C. elegans p38 MAPK pathway regulates nuclear localization of the transcription factor SKN-1 in oxidative stress response, Genes Dev. 19 (2005) 2278–2283, https://doi.org/10.1101/gad.1324805.
[69] C.C. Hsieh, M. Kuro-o, K.P. Rosenblatt, R. Brobey, J. Papaconstantinou, The ASK1-Signalosome regulates p38 MAPK activity in response to levels of endogenous oxidative stress in the Klotho mouse models of aging, Aging (Albany NY) 2 (2010) 597–611, https://doi.org/10.18632/aging.100194.